Next Sustainability 3 (2024) 100029

Contents lists available at ScienceDirect

Next Sustainability

journal homepage: www.sciencedirect.com/journal/next-sustainability

Review article

Alternate water electrolysis

Yao Chen [a], George Zheng Chen [b,*]

[a] The State Key Laboratory of Refractories and Metallurgy, Faculty of Materials, Wuhan University of Science and Technology, Wuhan 430081, China
[b] Department of Chemical and Environmental Engineering, Faculty of Engineering, University of Nottingham, Nottingham NG2 7RD, UK

ARTICLE INFO

Keywords:
Water electrolysis
Alternate
Decoupling
Redox mediums
HER
OER

ABSTRACT

Hydrogen gas is a net zero carbon emission clean fuel with an unmatched high specific energy. Water electrolysis is an important alternative method to produce hydrogen to the traditional fossil hydrocarbon reforming in industry. The main challenges of water electrolysis are the high energy consumption (ca. 5 kWh m^{-3} (H_2) at 80 ℃) and, if accidentally formed, the explosive nature of any unintended mixing of the produced hydrogen and oxygen gases. In order to solve these problems, alternate water electrolysis has been developed by, for example, decoupling of the hydrogen evolution reaction (HER) from the oxygen evolution reaction (OER) in space or time. This critical review intends to introduce the concept and recent developments of alternate water electrolysis in different schemes, including the alternate thermolysis and electrolysis of water, the alternate water electrolysis by using a liquid or solid redox intermedium and the alternate half-electrolysis of water. All the alternate water electrolysis methods solve the gas mixing problem whilst half-electrolysis and those with a solid redox medium omit the membranes. Specifically, only the alternate half-electrolysis of water can save the energy consumption without compromising the operation life and production rate.

1. Introduction

Global energy consumption rises for the economic growth and the increased population. Approximately 36 billion tons of carbon dioxide (CO_2) are emitted into the atmosphere every year to meet the energy demand [1]. Hydrogen gas (H_2) is a net zero carbon emission fuel without any pollutants and greenhouse gases because its combustion produces only heat and water steam. It has the highest specific energy of 143 MJ kg^{-1} or 39.4 kWh kg^{-1} (HHV) among all fuels [2]. Despite the high abundance of hydrogen in the universe, it is seldomly available as an elementary substance on the earth. At present, H_2 is mostly commercially produced from fossil fuels by thermochemical processes, including hydrocarbon reforming and pyrolysis, which requires the container to withstand high temperature and further separation for purification [3]. Besides thermochemical processes of hydrocarbons, electrolysis can also produce H_2 and the oxygen gas (O_2) from water which is the most abundant natural resource. Broadly, water electrolysis has the advantages of high yields and purity [4]. The main challenges of water electrolysis are the high energy consumption (ca. 5 kWh m^{-3} (H_2) at 80 ℃) [5]. The discovery of the water electrolysis can be dated back to 1789 when Deiman and Troostwijk used an electrostatic generator as the direct current source to decompose water into H_2 and O_2 in a Leyden jar [6,7]. Nowadays, water electrolysis driven by energy from renewable sources such as solar, wind and tide enable the scale-up of onsite H_2 production with net zero CO_2 emissions, meanwhile alleviating the instability of grid because the power from renewable energy sources is intermittent [8,9]. Especially, H_2 as an energy carrier can be produced by solar-energy-driven electrolysis of water during the day and supply electrical power at night by for example fuel cells [10]. Therefore, water electrolysis has a promise to take the place of thermochemical processes of hydrocarbons in the near future [11].

Conventionally, the overall cell reaction of water electrolysis can be divided into two half-cell reactions, comprising hydrogen evolution reaction (HER) at the cathode and oxygen evolution reaction (OER) at the anode. Take acidic electrolytes as an example, the total HER process represented by Eq. (1) could be divided into the Volmer, Heyrovsky and Tafel steps shown in Eqs. (2)–(4), respectively. The kinetic steps in the overall OER process of Eq. (5) should include Eqs. (6)–(9).

$$2H^+ + 2e = H_2\uparrow \quad (1)$$

$$H^+ + * + e = H^* \quad (2)$$

$$H^* + e + H^+ = H_2\uparrow \quad (3)$$

* Corresponding author.
E-mail address: george.chen@nottingham.ac.uk (G.Z. Chen).

https://doi.org/10.1016/j.nxsust.2024.100029
Received 15 December 2023; Received in revised form 6 February 2024; Accepted 15 February 2024

$$2H^* = H_2\uparrow + 2* \quad (4)$$

$$H_2O - 2e = 2H^+ + \frac{1}{2}O_2\uparrow \quad (5)$$

$$H_2O + * - e = H^+ + OH^* \quad (6)$$

$$OH^* - e = H^+ + O^* \quad (7)$$

$$H_2O + O^* - e = OOH^* + H^+ \quad (8)$$

$$OOH^* - e = H^+ + * + O_2\uparrow \quad (9)$$

The theoretical decomposition voltage of water electrolysis is 1.23 V under standard conditions at 298 K [12]. The electrode involving OER dominates the cell overvoltage which must be applied practically in water electrolysis in addition to the theoretical value, because the overpotential of HER is much smaller. Based on the fact that the performance of water electrolysis is mainly limited by OER, most reported studies on water electrolysis focus on the catalysts for OER [13–17]. The mechanisms of HER and OER with catalysts based on density functional theory have been introduced in our recent review [18]. The current commercial water electrolysis instrument is alkaline water electrolysis (AWE), whilst the developments of proton exchange membrane electrolysis cell (PEMEC), alkaline anion exchange membrane electrolysis cell (AEMEC) and solid oxide electrolysis cell (SOEC) are also showing promising commercial values [19]. Thereinto, SOEC operates at high temperatures of 873–1273 K and others at ambient temperatures. Either the 20–30% KOH aqueous solution is used in AWE as electrolyte, or deionized water or steam is feed in membrane-based electrolysers and SOEC [20,21]. However, the scarcity of fresh water in some coastal arid zones of the world makes it more desirable to electrolyse seawater which accounts for 96.5% of total water on the earth [10,22]. Although the cost of direct seawater electrolysis in practice should be considered [23], H_2 from seawater is of particular interest to the marine industry because H_2 production at offshore wind and/or solar farms is competitive with direct electricity transmission to shore if the distance is beyond 50 km [24].

It is well known that in air, H_2 can explode in a wide concentration range from 4.0%–75.6%, which is of a high safety concern for storage and transport. High-purity H_2 is also needed for application in industrial processes or fuel cells. In order to avoid the mixing of simultaneously produced H_2 and O_2 in conventional water or steam electrolysis, the corresponding gas-proof but ion-conducting diaphragms or membranes are designed and installed to separate the anode from the cathode. For example, asbestos diaphragms are selected for AWE, proton exchange membranes (PEM) for PEMEC, anion exchange membranes (AEM) for AEMEC and yttria stabilized zirconia (YSZ) for SOEC. Even though, gases have a tiny rate to permeate the membranes due to the pressure difference between the anodic and cathodic chambers. When water electrolysis is driven by the intermittent renewable energy, especially solar electricity, the provided current may be extremely low to result in a low rate of gas production. If the rate of gas production is not at least an order of magnitude larger than the rate of gas permeation, the gases will be mixed and become explosive. Furthermore, such unwanted gas crossover could induce the production of reactive oxygen species which severely degrade electrolyser components and hence shorten the whole cell lifetime. Although the indispensable diaphragms and membranes can impede the gas crossover to some extent and even membranes can transport ions as electrolytes, the diaphragm and membranes engender at least four disadvantages. First, the diaphragm or membrane resistance gives rise to extra voltage loss and energy consumption especially when a large current is applied. Second, particular polymer membranes, such as PEM and AEM, are considerably expensive. Third, pressure balance between the anode and cathode confines the applied electrolysis current and rate. Last but not the least, either acidic or alkaline diaphragms do not simultaneously favour HER and OER.

In order to solve the problems caused by gas crossover and high energy consumption in conventional water electrolysis with or without using renewable energy, several alternate water electrolysis strategies have been proposed. Such approaches aim to separate or decouple the HER and OER in space and/or time, particularly in the absence of diaphragms or membranes, as demonstrated in laboratory [25–29]. This critical review intends to introduce the concept and development of various alternate schemes for water decomposition, including alternate thermolysis and electrolysis of water, alternate water electrolysis via a liquid or solid redox medium, and alternate half-electrolysis of water. The relations and differences among these schemes are also revealed and compared. Finally, this review forecasts the promise and trend of these schemes of alternate water electrolysis in the context of practical applications.

2. Alternate thermolysis and electrolysis of water

Not only electrolysis but also thermolysis can split water into H_2 and O_2 [30]. Thermolysis of water can proceed at high temperatures (above 3000 K) which can be achieved via properly concentrated sunlight with potentially low or no greenhouse gas emissions. Water thermolysis seems to have nothing to do with alternate water electrolysis, but the decoupling of H_2 and O_2 was proposed in 1966 by multistep thermochemical processes with oxides as redox mediums [31]. It is possible to operate a sequence of thermochemical steps at temperatures well below the temperature required for water decomposition in a single step [32]. Fe_3O_4/FeO [33], ZnO/Zn [34] and CdO/Cd [35] as redox mediums were attempted to decouple H_2 and O_2 in the field of solar thermolysis. Taking CdO/Cd as an example, Eq. (10) produces O_2 whilst Eq. (11) produces H_2.

$$CdO = Cd\uparrow + \frac{1}{2}O_2\uparrow \quad (10)$$

$$Cd + H_2O = CdO + H_2\uparrow \quad (11)$$

However, for the chemical reaction step in Eq. (11), passivation caused by the formation of an oxidised upper layer makes it necessary to be carried out in an electrolyser. In 1983, solar energy was applied to decompose CdO at 1900 K under an Ar atmosphere, thereby producing a metallic Cd anode for the water electrolysis in which H_2 was produced. In other words, Eq. (11) turned from a thermochemical reaction to an electrochemical reaction. Unfortunately, the cycle efficiencies were as low as near 10%, partly because the Cd vapor needs to be separated from the co-product O_2 due to the higher temperature required to reduce CdO, well above the boiling point of Cd metal (1040 K).

In 2012, the concept was proposed that thermolysis combined with electrolysis using a metal oxide anode to decouple H_2 and O_2 [36]. Compared with the metal anode, like Cd [35], metal oxide anode in the electrolysis process increased the cycle efficiencies to above 60%, making solar-thermally decoupled water electrolysis towards practical development [36]. Taking Fe_2O_3(FeOOH)/Fe_3O_4 as an example, Eq. (12) produces O_2 in the air by solar thermolysis at 1650 K, whilst Eqs. (13) and (1) produce H_2 by electrolysis, as shown in Fig. 1a.

$$3Fe_2O_3 = 2Fe_3O_4 + \frac{1}{2}O_2\uparrow \quad (12)$$

$$2Fe_3O_4 + 4H_2O - 2e = 6FeOOH + 2H^+ \quad (13)$$

Firstly, because the water electrolysis step corresponding to Eqs. (13) and (1) can be decoupled in time from the solar step, this whole process is possible to be 24-hourcontinuous, showing an advantage compared with solar thermolysis of water decoupled by thermal chemical reactions. Secondly, the solar-heat-driven metal oxide reduction in Eq. (12) can be accomplished in air at temperatures below 1700 K, avoiding a window-closed reactor which incurs efficiency loss via transmission applied in metal oxide reduction to metal, as shown in Eq. (10) in Ar or

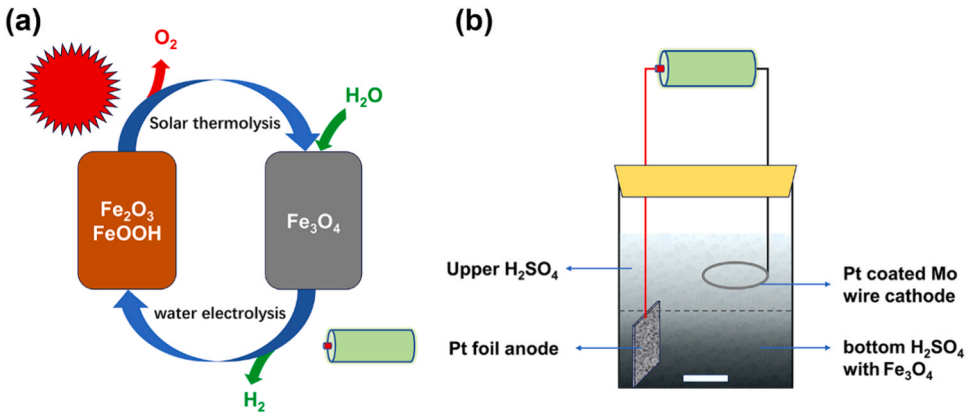

Fig. 1. Schematic illustration of (a) solar-heat decoupled water electrolysis process and (b) electrolyser part [36].

at a reduced pressure. Furthermore, the relatively low temperatures solve the challenges of material degradation. Thirdly, the theoretical minimum voltage to trigger Eqs. (13) and (1) is only 0.23 V at 298 K, which is much smaller than 1.23 V for water electrolysis because oxides are produced instead of encountering the sluggish OER at the anode. Concretely, after solar thermolysis of Fe_2O_3 in Eq. (12) to release O_2, the resulting Fe_3O_4 was placed in either H_2SO_4 or KOH supporting electrolytes. The appropriate stirring rate compromised the gravity of the Fe_3O_4 particles to deliberately maintain two regions in the electrolytes: the bottom region contained suspended Fe_3O_4 particles whilst the upper part was of the supporting electrolytes without particles, as illustrated in Fig. 1b. The cathode was a Pt-coated Mo wire placed in the upper electrolyte for HER, avoiding the disturbance of Fe_3O_4 particles. The anode was a Pt foil electrode inserted into the bottom suspension region of the electrolytes for catalysing the oxidation of the Fe_3O_4 particles. The gas chromatography analysis of the headspace of the cell did not detect O_2, suggesting that the decoupling of the HER from OER was realised. After the unreacted magnetite Fe_3O_4 particles were separated from the product using magnets, the remaining yellow powder in electrolyte was demonstrated to be FeOOH by X-ray diffraction. In fact, Fe_2O_3 is the dehydration product of FeOOH, and hence the cycle can be completed. The electrolysis current of the system in H_2SO_4 electrolyte was much higher than that in KOH because the Fe_3O_4 particles can be, at least partly, a solute in acidic electrolytes. It is worth noting that the initial voltage decreased from about 1.8 V for conventional water electrolysis with Pt as the anode to 0.7 V when the Fe_3O_4 particles were used as the anode. The maximum possible thermal efficiency obtained was above 60% when the only thermal input not recovered is that required to drive the reduction reaction, implying solar-heat decoupled water electrolysis to be a promise in practical application. Subsequently, extended research on the anodic electrochemical reaction with the Co_3O_4/CoO redox medium was also investigated [37].

It is worth referring to the report in 2020 that microwave heating could decouple water thermolysis on $Ce_{0.8}Gd_{0.2}O_{1.9}$ at temperatures below 250 °C which would save much energy [38].

The decoupling of H_2 and O_2 was actually proposed initially for solar thermolysis of water in multistep thermochemical processes with oxides as the redox mediums or via the combination of solar thermolysis and electrolysis with oxides/metal as redox mediums. However, the work on solar-heat decoupled water electrolysis with a low valence metal oxide as the anode has demonstrated that it can be possibly realised in practical applications. This is because not only does the maximum ideal efficiency reach beyond 60%, but also the solar thermolysis can be executed at a relatively low temperature in air.

3. Alternate water electrolysis by liquid redox medium

Compared with solar thermolysis of water, water electrolysis can be operated at room temperature and low temperature, which does not require solar heating instruments. In water electrolysis systems, on the one hand, industrial processes and fuel cells require sufficiently pure H_2, whilst on the other hand, the kinetics of OER are too sluggish to keep pace with that of HER. Hence, it would be wonderful if the evolved H_2 and O_2 in water electrolysis are produced separately in time or space. As we know, natural photosynthetic systems are able to split water to produce only O_2 coupled with protons which support the conversion from adenosine diphosphate to adenosine triphosphate [39,40]. As mentioned in the last session, solar thermochemical cycles of water splitting may produce H_2 and O_2 at separate times on a large scale.

3.1. Electron-coupled proton buffer

Inspired by these findings, in 2013, it was proposed that an electron-coupled proton buffer (ECPB) could be applied to decouple HER and OER during water electrolysis [41]. Commercially available phosphomolybdic acid $(H_3O)^+[H_2PMo_{12}O_{40}]^-$, a type of yellow polyoxometallic acid with a pH of 0.3, was chosen to be the ECPB. It possesses peculiar properties, such as high solubility in water, high storage capacity for protons and electrons, at least one reversible redox peak between HER and OER, and the capability to accept charge-balancing protons when it is reduced to buffer the pH of the solution. These properties are criteria when developing a new ECPB. The phosphomolybdic acid $(H_3O)^+[H_2PMo_{12}O_{40}]^-$ exhibited four pairs of redox peaks in cyclic voltammogram (CV). The first reduced state of $(H_3O)^+[H_2PMo_{12}O_{40}]^-$ in aqueous solution was the two-electron reduced species $(H_3O)^+[H_4PMo_{12}O_{40}]^-$. The decoupling of HER and OER with the ECPB was demonstrated in a Nafion membrane separated cell consisting of two compartments, one filled with 1 mol L^{-1} H_3PO_4 and the other with a 0.5 mol L^{-1} mixture of $(H_3O)^+[H_2PMo_{12}O_{40}]^-$ and $(H_3O)^+[H_4PMo_{12}O_{40}]^-$ (1:1) and two Pt electrodes. Fig. 2 illustrates the entire process of decoupling HER and OER with ECPB. The first step involved the oxidation of water to produce O_2 by the reduction of yellow $(H_3O)^+[H_2PMo_{12}O_{40}]^-$ to dark blue $(H_3O)^+[H_4PMo_{12}O_{40}]^-$, as shown in Eqs. (14) and (5). In the second step, when the dark blue $(H_3O)^+[H_4PMo_{12}O_{40}]^-$ was reversibly oxidised to the yellow $(H_3O)^+[H_2PMo_{12}O_{40}]^-$, H_2 was evolved in the H_3PO_4 chamber which was the same one where OER occurred in the first step, as written in Eqs. (15) and (1). The two steps with ECPB could be continuously cycled to complete the alternate water electrolysis.

$$(H_3O)^+[H_2PMo_{12}O_{40}]^- + 2H^+ + 2e = (H_3O)^+[H_4PMo_{12}O_{40}]^- \quad (14)$$

$$(H_3O)^+[H_4PMo_{12}O_{40}]^- - 2e = (H_3O)^+[H_2PMo_{12}O_{40}]^- + 2H^+ \quad (15)$$

From Eqs. (14) and (5), it is worth paying attention that phosphomolybdic acid can store both the protons and the electrons generated during water oxidation. It acted to buffer the pH in the electrolysis cell,

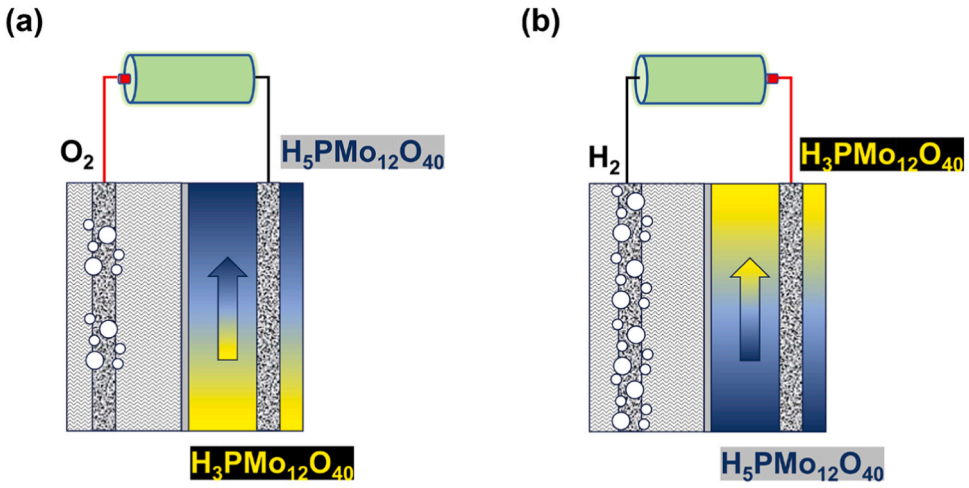

Fig. 2. Schematic illustration of ECPB decoupled water splitting. (a) OER along with reduction of phosphomolybdic acid and (b) HER with oxidation to phosphomolybdic acid. Copyright Nature Springer 2013 [41].

which would be benefit for the durability of water electrolysis. That is why it was called ECPB, as it maintained an unchanged pH. If it was changed to a polyoxometalate of $Na_4(NH_4)_2[H_2VW_{17}O_{54}(VO_4)_2]$ with a pH of 3.67, the pH of the counter chamber containing Na_2SO_4 changed from 3.67–11.96, which was close to that expected by calculation, after the reduction of water to H_2 and oxidation of $Na_4(NH_4)_2[H_2VW_{17}O_{54}(VO_4)_2]$. The pH change occurred because there were not sufficient H^+ provided from polyoxometalate to release H_2, which must be formed from H_2O with OH^-. This may indicate that the polyoxometalate is not suitable to be an ECPB. The porous frit was also applied in the phosphomolybdic acid system instead of a Nafion membrane to compare the pH changes. Furthermore, the Fe^{2+}/Fe^{3+} and I_2/IO_3^- couples, which were used as redox mediums in artificial photosynthetic Z-scheme systems, were proved to be unsuitable to be ECPB. Too small ionic size, positively charged and unstable Fe^{2+} are reasons why the Fe^{2+}/Fe^{3+} couple should not be an ECPB. Besides buffering pH, the two-electron transferred phosphomolybdic acid possessed good stability. The reduced state of $(H_3O)^+[H_4PMo_{12}O_{40}]^-$ could be stored in an open container for at least two weeks with stirring.

Owing to almost unchanged pH in the phosphomolybdic acid system, potential losses could be ignored especially when compared with the potential drop from solution resistance. When considering the conventional water electrolysis coupling of OER and HER as a benchmark, the overall energy consumption of the alternate two-step process in the two-electrode cell was 1.27 times that of the one-step conventional electrolysis, meaning that the alternate water electrolysis consumed more energy.

3.2. Spontaneous catalysis

Subsequently, another cheaper polyoxometallic acid, silicotungstic acid, was attempted to be used as an ECPB [42]. The CV showed that $H_4[SiW_{12}O_{40}]$ had two reversible redox peaks at 0.01 and –0.22 V versus the normal hydrogen electrode (NHE) using a glassy carbon electrode, which were far more positive than –0.6 V, the onset of HER on a glassy carbon electrode in a similar pH electrolyte absence of $H_4[SiW_{12}O_{40}]$. However, when a Pt electrode was used as in the previous report [41], competitive reactions between HER and the reduced mediator occurred, generating a mixture of $H_4[SiW_{12}O_{40}]$ and its one-electron reduced form of $H_5[SiW_{12}O_{40}]$. In the first step of the alternate water electrolysis, $H_4[SiW_{12}O_{40}]$ was reduced to dark blue $H_6[SiW_{12}O_{40}]$ via a carbon felt cathode whilst OER occurred at a Pt anode. The two-electron reduction of $H_4[SiW_{12}O_{40}]$ could be completed with only trace H_2, indicating that the decoupling of HER and OER would be successful. It was supposed to alter the anode and cathode to execute the second step. Fortunately, it was surprising that when the Pt/C catalyst was inserted into the reduced state $H_6[SiW_{12}O_{40}]$, HER spontaneously occurred, as shown in Fig. 3. The mechanism of the spontaneous HER was similar to that of the chemical heterogeneous catalysis with noble catalysts [43,44]. The decoupling by electrolysis and chemical catalysis realised the separation of HER and OER in time and space and showed many advantages as follows. Firstly, the electrochemical setup, at least the anodic compartment, could be open in the ambient environment if we need not O_2. Secondly, the reduced state $H_6[SiW_{12}O_{40}]$ could be transferred to a separate chamber to perform spontaneous HER at elevated temperature and pressure to increase the production rate freely. Thirdly, reactive oxygen species, which would result in the degradation of membranes, produced by the coexistence of H_2 and O_2 were thoroughly avoided. Finally, H_2 would be highly pure because any residual O_2, if present, would react with the reduced mediator in the separate chamber, rendering the H_2 suitable for applications in fuel cells or the Haber-Bosch process.

Further investigation on the purity and rate of H_2 was carried out.

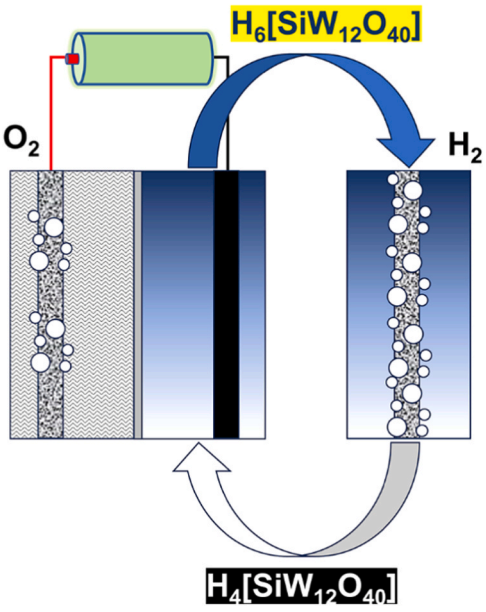

Fig. 3. Schematic illustration of silicotungstic acid-mediated decoupling OER and spontaneous HER [42].

When 10% O_2 was deliberately inflated into the headspace of $H_6[SiW_{12}O_{40}]$, only 0.04% O_2 left by the reaction with $H_6[SiW_{12}O_{40}]$ after 30 min, further guaranteeing the purity of H_2. The rate per milligram of Pt from $H_6[SiW_{12}O_{40}]$ exceeded that in the PEMEC by a factor of 30 [45]. The released volume of H_2 ranged between 122.4 and 244.7 mL, corresponding to one and two-electron conversions, respectively. The faradaic efficiency was 68% relative to the two-electron reaction. This means that complete and rapid transformation of $H_6[SiW_{12}O_{40}]$ to $H_5[SiW_{12}O_{40}]$ was followed by partial conversion of $H_5[SiW_{12}O_{40}]$ to $H_4[SiW_{12}O_{40}]$. The resulting mediator solution was titrated with an Fe(III) source to oxidize all remaining $H_5[SiW_{12}O_{40}]$ to colourless $H_4[SiW_{12}O_{40}]$. Another research [46] found that the yield of H_2 reached 85% over Pt/C subjected to the reduced silicotungstic acid in a water-ethanol solution because the addition of ethanol can increase the reducing capability of silicotungstic acid.

The spontaneous HER was indeed an intriguing phenomenon and realised the separation of HER and OER both in time and in space, offering many advantages as mentioned above. It seems to be capable of omitting the purge of O_2 after OER in the alternate decoupling applied in the literature [41]. However, at least for $H_4[SiW_{12}O_{40}]$, there were still some problems. When OER occurred, a Pt electrode could not be used for the reduction of $H_4[SiW_{12}O_{40}]$, leading to the decreased electrocatalytic activity. After spontaneous HER, the oxidation of the residual $H_5[SiW_{12}O_{40}]$ required an extra step. In other words, in fact, the decoupling course had to undergo three steps, comprising OER by electrolysis, spontaneous HER and oxidation of the intermediate of the ECPB. Additionally, the molecular weight of $H_4[SiW_{12}O_{40}]$ is still too large to store hydrogen efficiently.

As a matter of fact, the concept of redox ECPB bears some resemblance to the mechanism of redox flow batteries. All-vanadium redox flow batteries, which use V(III)/V(II) and V(V)/V(IV) redox couples, have been commercialized [47]. Reported simultaneously with the spontaneous HER [42], both chemical catalysis reactions of HER and OER occurred spontaneously in different redox solutions charged by a conventional V–Ce redox flow battery, realizing the decoupling of water electrolysis [48]. The authors claimed that the dual circuit system could provide a secondary platform to store surplus energy beyond the capacity of the charged electrolytes in the form of hydrogen [48]. However, this is impossible because all energy, certainly including hydrogen, comes from the electrochemical conversion of the redox electrolyte ions. In fact, the mechanism of half of the dual-circuit system was similar to that described in the literature [42]. Fig. 4 illustrates the schematic of the dual-circuit system consisting of a redox flow battery and two catalytic beds, half of which is similar to Fig. 3.

A single V–Ce redox flow battery was designed, wherein pretreated graphite felt electrodes were utilised in 0.1 mol L^{-1} Ce(III) ($Ce_2(SO_4)_3$) and 0.1 mol L^{-1} V(IV) ($V(SO_4)_2$), converted to Ce(IV) and V(III), in 1 mol L^{-1} H_2SO_4, achieving mean charging and discharging cell voltages of 2.5 and 0.7 V at 60 mA cm^{-2}. However, the drawback of the redox flow battery was its low energy efficiency. In the catalytic beds, only pre-heated hydrated RuO_2 nanoparticles were active for OER in the electrolyte containing Ce(IV), whilst Mo_2C was employed as the catalyst for HER in V(II). Simple 3-way valves were utilised to control the electrolyte directions among the battery body, tanks and catalytic beds. The mean conversion efficiency of OER from Ce(IV) was 78%, indicating side reaction that hydrated RuO_2 was corroded by consuming the Ce(IV). The overall energy efficiency of the dual circuit system, the ratio between the energy "contained" in the produced hydrogen and the electrical energy required to fully charge the V–Ce redox flow battery, was about 50% at a charging current density of 60 mA cm^{-2}, considering the lower heating value for hydrogen (241 kJ mol^{-1}) and a HER yield of 100%.

Whether Figs. 3 or 4, at least one catalytic chamber was utilised to separate HER and OER in space. In Fig. 3, only a redox ECPB was used, whilst in Fig. 4, two different redox ion couples, even if all-vanadium ones, with a certain potential difference based on the concept of redox flow battery, must be utilised. In fact, the configuration in Fig. 3 can be seen as a simplification of that in Fig. 4, where the left parts of Fig. 4a and c become the electrolytic OER part in Fig. 3. Both configurations with different setups aim to achieve the decoupling of HER and OER in time and space.

3.3. Multielectron reactions

Although soluble redox mediators, such as phosphomolybdic acid

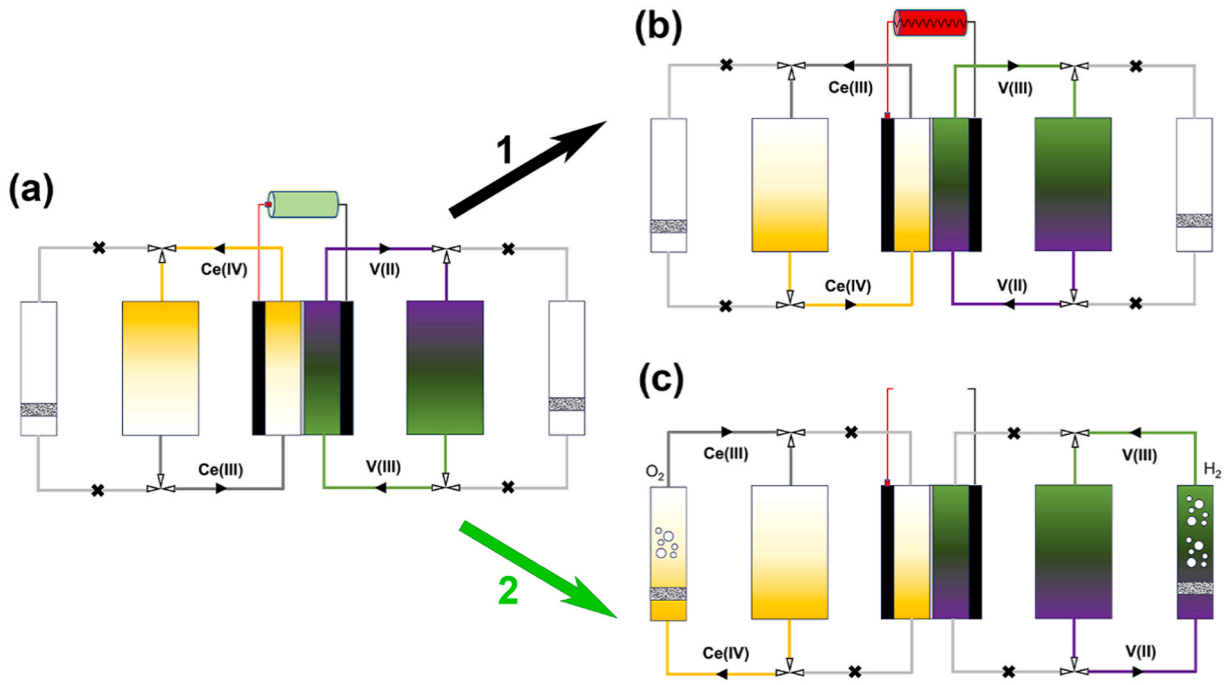

Fig. 4. Schematic illustration of dual circuit system from (a) charging to (b) discharging by redox flow battery via conventional route 1 or to (c) decouple HER and OER by catalytic beds via new route 2 [48].

and silicotungstic acid, were employed in decoupling HER and OER, the electron storage capacity of these mediators was limited to only 1 or 2 electrons per molecule. Polyoxometallates offer a tremendous ability to reversibly store multiple electrons. Small cations, such as Li^+, play a crucial role in reducing the redox potentials of polyoxometallates to facilitate the generation of reduced species, compared with those when these cations are absent [49]. Leveraging this significant advantage, polyoxometallates have been investigated in redox flow batteries [50]. $Li_6[P_2W_{18}O_{62}]$ polyoxometalate was chosen to decouple HER and OER as it is capable of reversibly accepting up to 18 protons and electrons in aqueous solution [51]. When the supporting electrolyte was 1 mol L^{-1} Li_2SO_4/H_2SO_4 with a pH of 4 and the concentration of $Li_6[P_2W_{18}O_{62}]$ increased to 0.1 mol L^{-1}, the current profoundly increased in CV and could deliver 17.2 electrons per molecule throughout the process practically. Combining the dual membrane design and the configuration of the redox flow battery (similar to Fig. 4), a tank with a pump was used to circulate the redox EPCB of $Li_6[P_2W_{18}O_{62}]$ between OER and HER membrane-based electrolysers, as depicted in Fig. 5.

In order to avoid competitive HER during the multielectron reduction of $Li_6[P_2W_{18}O_{62}]$, a high flow rate had to be utilised to minimize mass transport overpotentials. This is why a static electrolyser cannot be applied as depicted in Fig. 5. Such a high flow rate was applied in a similar configuration using silicotungstic acid as an ECPB which could confer greater tolerance to mineralized water [52]. However, the high flow rate entails high energy consumption in practical applications, which is often overlooked in energy calculations in most papers. When the reduced specimen of $[P_2W_{18}O_{62}]^{6-}$ by 18 electrons per molecule by the electrochemical flow was exposed to Pt/C, a 16-electron equivalent of H_2 was spontaneously generated, leaving behind a two-electron reduced anion of $[P_2W_{18}O_{62}]^{8-}$. More interestingly, spontaneous HER from solutions of the reduced specimen occurred without any bias and even without any catalyst. Simply diluting the solution with a higher pH Li_2SO_4, increased the kinetics of HER.

Another multielectron conversion of ECPB was explored by changing the heteroatom in silicotungstic acid from Si^{4+} to Zn^{2+}, which doubled the number of reversible electrons from two to four [53]. It was observed that $H_6ZnW_{12}O_{40}$ maintained a stable pH even when undergoing 4-electron reduction, which was markedly different from the significant pH change observed when reducing $H_4SiW_{12}O_{40}$. The CV peaks of $H_6ZnW_{12}O_{40}$ shifted to negative potentials with increased pH by adding buffering solutions, which was attributed to the enhanced protonation ability of $[ZnW_{12}O_{40}]^{6-}$ accompanying reduction in acidic solutions. The reduced specimen of $H_6ZnW_{12}O_{40}$ released 95.5% of the theoretical H_2 volume, significantly higher than the 67% for $H_6SiW_{12}O_{40}$. The authors stated that the incomplete release of hydrogen is caused by the first redox potential of $H_4SiW_{12}O_{40}$ being more positive than the HER onset potential of Pt/C catalyst. However, in fact, this is a chemical catalytic process rather than an electrocatalytic one, despite redox reactions occurring. The explanation of partial oxidation of $H_5SiW_{12}O_{40}$ to $H_4[SiW_{12}O_{40}]$ [42] appears to be more accurate.

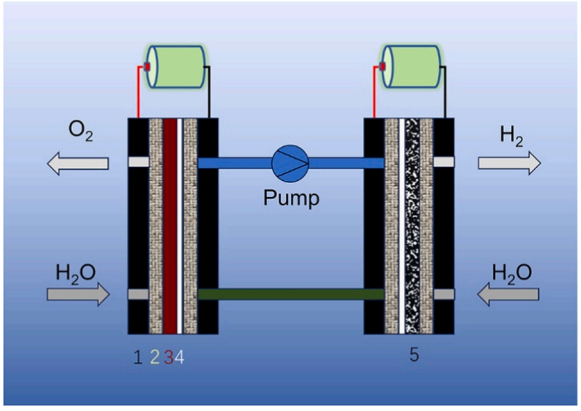

Fig. 5. Flow cell device to decouple HER and OER by the reduction and oxidation of $Li_6[P_2W_{18}O_{62}]$, from 1 to 5 correspond to flow channel, carbon paper, IrO_2 OER catalyst, Nafion membrane and Pt HER catalyst [51].

3.4. Organics

Considering that the molecular weight of the all-inorganic polyoxometalate phosphomolybdic acid ($H_3Mo_{12}PO_{40}$) as an ECPB is > 1800 g mol^{-1}, ECPBs with lower molecular weights along with characteristics of abundant components and industrial scale production are desired. Bionics offers a shortcut to find desired substances, thanks to the gifts of nature. Quinone derivatives, such as plastoquinone, are known to be mitochondrial redox carriers in natural photosynthesis in green plants. Plastoquinone can accept electrons from Photosystem II during water oxidation and protons from the chloroplast stromal matrix, undergoing a reversible two-electron transfer process to form a reduced hydroquinone derivative. These electrons and protons stored in the hydroquinone derivative are ultimately used to yield NADH, an H_2 equivalent if applied in water electrolysis, from NAD^+ [54]. Inspired by plastoquinone in natural photosynthesis, commercially available 1,4-hydroquinone derivative potassium hydroquinone sulfonate is selected to be an ECPB [55]. The linear scanning voltammogram (LSV) showed a much lower onset voltage in the potassium hydroquinone sulfonate system than that in the pure H_3PO_4 system, whether for HER or OER. However, cyclic performance showed that the ability to re-reduce potassium hydroquinone sulfonate decreased by 1% per cycle. This extension of ECPB from inorganic large molecules to organic small molecules is promising, however, the reversibility of potassium hydroquinone sulfonate should be improved.

In order to alleviate the degradation of potassium hydroquinone sulfonate (1% per cycle), anthraquinone-2,7-disulfonic acid which demonstrated impressive reversibility as the negative electrolyte in a redox flow battery, was chosen as the ECPB. The charge capacity exhibited an overall decrease of 5.75% over 100 cycles, corresponding to 0.06% per cycle [56], which was one 17th of that observed with potassium hydroquinone sulfonate.

3.5. Photocatalysis

As we know, solar energy has long been applied in water splitting, where catalysts in the anode must be photoactive semiconductors with energy gaps smaller than the energy of photons [57–59]. Recently, a photoanode of WO_3 was utilised as the catalyst to decouple HER and OER in a photoelectrochemical cell. A dual membrane cell was designed to separate HER and OER in different chambers, with phosphomolybdic acid still serving as the redox ECPB (Fig. 6) [60]. This design is a modification of that shown in Fig. 2, enabling the separation of HER and OER in space, albeit with the addition of an extra PEM, thereby increasing the cost of the decoupling system. The WO_3 photoanode in 1 mol L^{-1} CH3SO3H facilitated the simultaneous oxidation of water to

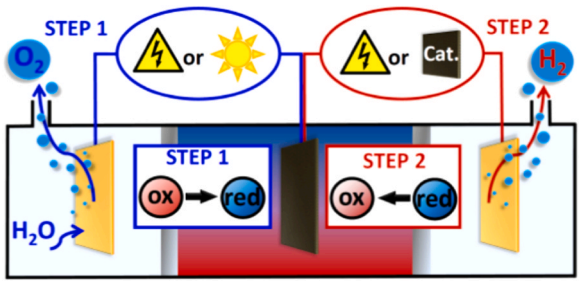

Fig. 6. Schematic illustration of dual membrane photoelectrochemical cell to decouple OER with WO_3 photoanode by step 1 and HER by step 2 in space with ECPB [60].

O_2 in the photoanode chamber and the reduction of $[PMo_{12}O_{40}]^{3-}$ to $[PMo_{12}O_{40}]^{5-}$ in the middle chamber via an external circuit without any additional electric bias. The achieved current densities were over 1 mA cm^{-2} under simulated solar irradiation, with a faradaic efficiency for OER in photolytic water splitting was 84%.

It was found that a WO_3 photoanode could be decomposed to tungsten acid upon contact with acidic $H_3PMo_{12}O_{40}$ during photoelectrochemically decoupled water splitting. $BiVO_4$ crystal is also an n-type photocatalyst with a 2.3 eV bandgap [61], making it a suitable photocatalyst for OER. In the initial step, under light irradiation, water was oxidised to oxygen by the photogenerated holes from the $BiVO_4$ powder in the $H_3PMo_{12}O_{40}$ solution, whilst the protons and electrons were stored in the ECPB, generating $H_5PMo_{12}O_{40}$. In the second step, the oxidised ECPB obtained in the first step was transferred to the electrolyser and reduced to $H_3PMo_{12}O_{40}$, concurrent with HER [62]. However, the deep colour of $H_3PMo_{12}O_{40}$ at high concentration hindered the light absorption of $BiVO_4$, thus limiting the efficiency of OER.

The (010) facets of $BiVO_4$ are known to be efficient for the reduction reaction, whilst the (110) facets are more conducive to the oxidation reaction [63]. The $BiVO_4$ crystals with different ratios of (110)/(010) facets could be prepared by hydrothermal method at varying pH levels. The optimized areal ratio of (110)/(010) for photocatalytic activities was found to be 3, proving that the kinetics of reduction reaction are faster than that of the water oxidation reaction. The apparent quantum efficiency reached 71% at 365 nm, significantly higher than that of irregular crystals. Utilizing regular $BiVO_4$ crystals as the photocatalyst, decoupling HER and OER was achieved with the redox Fe^{2+}/Fe^{3+} couple ions [64]. The mechanism was similar to that illustrated in Fig. 6 but with a different photocatalyst and redox medium. The regular $BiVO_4$ crystals catalysed the oxidation of water with complete reduction of Fe^{3+} to Fe^{2+}. Conversely, the irregular $BiVO_4$ crystal exhibited unwanted reversible conversion of Fe^{2+}/Fe^{3+}, resulting in the decreased faradaic efficiency of OER. Photogenerated electrons and holes were spatially separated over the regular $BiVO_4$ crystal. After that, photogenerated electrons accumulated on (010) facets whilst holes (110) facets. Therefore, the regular facets facilitated the reduction of Fe^{3+} ions by photogenerated electrons and OER by photogenerated holes. In the electrolysis part, a bias of 0.8 V was applied to produce H_2 with oxidation of Fe^{2+}. Considering the redox potential of Fe^{3+}/Fe^{2+} was 0.77 V, the small overpotential of only 0.03 V indicated efficient electrolysis.

3.6. Base acid hybrid

As we well know, the potentials for OER and HER tend to decrease with an increase in the pH value of an electrolyte solution. Combining the high HER potential in an acidic electrolyte solution with the low OER potential in a basic electrolyte solution, the overall voltage of water splitting would be lower than 1.23 V. However, achieving such a setup is challenging due to the difficulty of maintaining the coexistence of an acid and a base in an electrolytic system. The use of a bipolar membrane has emerged as a potential solution to this challenge, which comprises cation-selective face and the anion-selective face, allowing for the separation of acidic and basic electrolytes [65]. Recently, the ceramic Li-ion exchange membrane was used to separate basic and acidic electrolytes in water electrolysis [66]. In the setup, a commercial bipolar membrane was used to separate 0.36 mol L^{-1} $V_2(SO_4)_3$ in H_2SO_4 from KOH. A polycrystalline Si photovoltaic module powered the electrolysis which decoupled OER in the basic electrolyte concurring the reduction of V^{3+} to V^{2+}. The voltage drop across the bipolar membrane was 0.866 V, which includes a concentration polarization effect between different pH environments, at a current density of 10 mA cm^{-2}. When a 96% V^{2+} solution was passed to Mo_2C catalysts, spontaneous HER occurred with a faradaic efficiency of 83% [67]. The designation was similar with that in Fig. 3 but applying a bipolar membrane with different pH electrolytes. Noting that although the electrolysis was driven by solar energy, it is completely different from the photocatalysis.

The progress on bipolar membranes is still on the phase of research and development. Nevertheless, bipolar plates are commercially used to connect individual fuel cells and electrolysers in stacks. Alternate water electrolysis by stepwise operations requires more time compared with conventional water electrolysis, despite its ability to prevent the mixing of H_2 and O_2 gases. Inspired by bipolar plates used in cell stacks, electrically connected bipolar electrodes were employed to contact two separate redox solutions of $K_3Fe(CN)_6/K_4Fe(CN)_6$ in 0.1 mol L^{-1} KOH. Fig. 7 shows the configuration of the bipolar electrode system. In this setup, the anodic and cathodic reactions of the redox solutions occurred simultaneously, leading to synchronous HER and OER on the opposite sides of PEMs in the two compartments [68]. To operate the device continuously as a water electrolyser, the anode and cathode must be periodically switched to maintain the pH of the electrolytes and regenerate the redox solutions. Therefore, despite the advantages, the need for purging between alternate steps remains unavoidable. It is doubtful whether PEMs employed in the alkaline supporting electrolytes was appropriate. Since HER and OER occurred at separate compartments, basic and acidic electrolytes could be utilised in the water electrolysis, which, although was not done, was demonstrated by the subsequent the research of the reverse fuel cells with the same configuration with bipolar electrodes.

Since HER and OER could be decoupled into two electrolysis parts like Fig. 5, attempts were made to conduct HER and OER in acidic and basic electrolytes, respectively. The V(II)/V(III) couple electrolyte served as the mediator was placed in a tank between the HER and OER electrolysis cells. The Ni foams were used as electrodes in both the HER and OER sides. Unfortunately, the Ni foam underwent the corrosion from the H_2SO_4 electrolyte in the electrochemical environment, increasing the cell voltage of HER with cycles. Both membranes in the HER and OER cells were AEMs which separated the V(II)/V(III) redox and H_2SO_4 and V(II)/V(III) redox and KOH, respectively [69]. The pH and absolute value of the voltage rapidly increased with stepwise electrolysis time on the OER side. Only by significantly increasing the amount of KOH could mitigate the pH change. It is noted that PEM cannot be employed even if in the HER cells with acidic cathode electrolyte because the PEM cannot prevent the outflow of the vanadium cations to the HER side. However, the degradation of AEM in the OER part was obvious because a large quantity of hydrated SO_4^{2-} species with a large ionic radius of 2.32 Å were transported through AEM due to a large concentration difference at the basic KOH–acidic vanadium solution interface. Furthermore, authors may have overlooked the fact that the amount of soluble vanadium cations would decrease if the OH^- ions from the OER side permeated to the V(II)/V(III) redox side to precipitate the vanadium ions. The AEM degradation led to the outflow of the vanadium cations and hence decrease the duration of each HER and OER with cycles. The cell voltage increased suddenly at the end of each HER

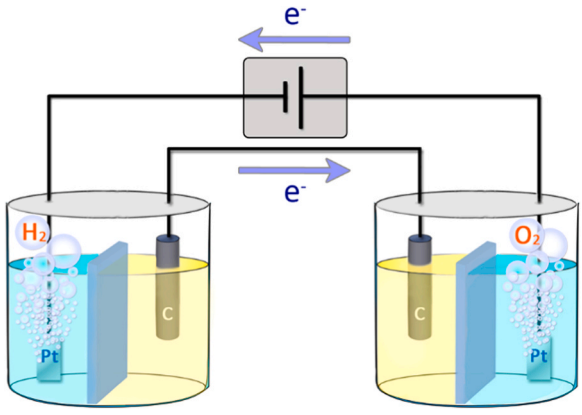

Fig. 7. Separation of simultaneous HER and OER in water electrolysis with electrically connected bipolar electrodes [68] (Copyright 2017, ACS).

and OER due to the unfavorable side reactions, including the oxidation of V^{3+} to V^{4+} and the reduction of H^+ to H_2, after the vanadium cations were completely converted, respectively.

From the two examples, at least three severe problems need to be addressed in the base acid hybrid alternate water electrolysis. Firstly, the voltage drop across the membrane due to the concentration difference between the basic and acidic electrolytes increases energy consumption, which should be offset by the ideal potential difference between HER in acidic and OER in basic electrolytes. Secondly, the dramatic change in pH after consuming the electrolyte would decrease catalytic activity. Thirdly, the specific membranes are more prone to degradation.

3.7. Non-alternate

Considering that the kinetics of OER are sluggish, other oxidation reactions like oxidation of 5-hydroxymethylfurfural (HMF) to value-added 2,5-furandicarboxylic acid (FDCA) requiring less positive potential could replace OER, which can not only save the energy but also avoid the mixture of H_2 and O_2 [70,71]. When $Na_4[Fe(CN)_6]$ was used as the redox medium, the decoupling of HER and the oxidation of HMF to FDCA could be achieved [72].

All-vanadium dual circuit redox flow battery could also be applied to decouple HER and OER. The reduction of V(V) to V(IV) [73] replaced the part of Ce(IV) to Ce(III) [48]. The reduction of V(V) to V(IV) could be matched with the oxidation of SO_2 gas to power a cell, instead of releasing O_2.

Another work also employed the configuration of a redox flow battery with iron triethanolamine (Fe(III)TEA) and K_2MnO_4 in an alkaline supporting electrolyte to induce HER spontaneously with the Pt/C catalyst in its reduced state (Fe(II)TEA). On the K_2MnO_4 side, no OER occurred. It can be inferred that the oxidation of K_2MnO_4 to $KMnO_4$ replaced OER by electrolysis [74].

There is no doubt that substituting another oxidation reaction for the sluggish OER can reduce the voltage of the entire cell. It is even more advantageous when the oxidation reaction is urgently useful and can even generate electricity. However, the reduced specimen must be continuously supplied, which is much more expensive, or at least more troublesome, than using water. Additionally, the pH on the oxidation side cannot be buffered, which would decrease catalytic activity over cycles. Therefore, alternate water electrolysis remains the primary method for producing pure H_2.

4. Alternate water electrolysis by solid redox electrode

The ECPBs used to decouple HER and OER in Session 3 are soluble redox ions in liquid phases. In principle, as long as redox reactions can occur, it is possible to use them to realize alternate water electrolysis.

4.1. $Ni(OH)_2$

$Ni(OH)_2$ has been widely used as the electrode material in alkaline aqueous rechargeable batteries [75]. Its charging and discharging courses depend on the reversible transformation between $Ni(OH)_2$ and NiOOH. $Ni(OH)_2$ as the redox medium completed the separation of HER and OER in alkaline water electrolysis in 2016. To enhance the electric conductivity and cyclic ability of $Ni(OH)_2$, carbon nanotubes (CNTs) were introduced, constituting 30% of the composite. Additionally, 10 wt % acetylene black was used as a conductive agent during electrode preparation. In fact, the real active component of $Ni(OH)_2$ accounted for about 60%. In the first step, $Ni(OH)_2$ was oxidised to NiOOH, whilst HER occurred simultaneously. In the second step, NiOOH was reduced to $Ni(OH)_2$ whilst OER occurred concurrently, as shown in Fig. 8a [76]. The corresponding electrochemical reactions are shown in Eqs. (16)–(19).

$$2Ni(OH)_2 + 2OH^- - 2e = 2NiOOH + 2H_2O \quad (16)$$

$$2H_2O + 2e = H_2\uparrow + 2OH^- \quad (17)$$

$$2NiOOH + 2H_2O + 2e = 2Ni(OH)_2 + 2OH^- \quad (18)$$

$$2OH^- + 2e = \frac{1}{2}O_2\uparrow + H_2O \quad (19)$$

The separation of HER and OER in time prevented the mixing of gases. More importantly, diaphragms or AEMs can be omitted because the redox medium was a solid electrode which generally could not flow to influence the HER or OER on the other side. Visually, having no membrane reduced the cost of the alkaline electrolyser. The cell voltage for HER exhibited a cell voltage of about 1.6 V at 20 mA cm^{-2} with the commercial Pt coated Ti mesh, derived from the potential difference between Eqs. (16) and (17) and that for OER −0.4 V (assuming $Ni(OH)_2$ always as the working electrode) with the commercial RuO_2/IrO_2 coated Ti mesh, derived from the difference between Eqs. (18) and (19). The energy consumption of the two-step water electrolysis using these precious electrodes was 1.09 times that of conventional water electrolysis, estimated by mean values of voltages, assumed to be close to the more accurate integration. Slight self-discharge was found during the rest between HER and OER, during which purging was carried out. The faradaic efficiency of HER was 94.7%.

As H_2 is more desirable than O_2 for the energy society, OER in the aforementioned Step 2 was replaced by the discharge of the (−) Zn | 1 mol L^{-1} KOH | NiOOH (+) battery (Fig. 8b). As the discharge product of the battery is $Ni(OH)_2$ and ZnO_2^{2-}, as shown in Eqs. (18) and (20), a circuit can be established between the HER and discharge of the battery. Although energy was saved by adopting the discharge of the battery instead of OER, the same problems may be of concern, as mentioned at the end of Session 3, in addition to the passivation and dendrite growth of the Zn electrode in practical applications.

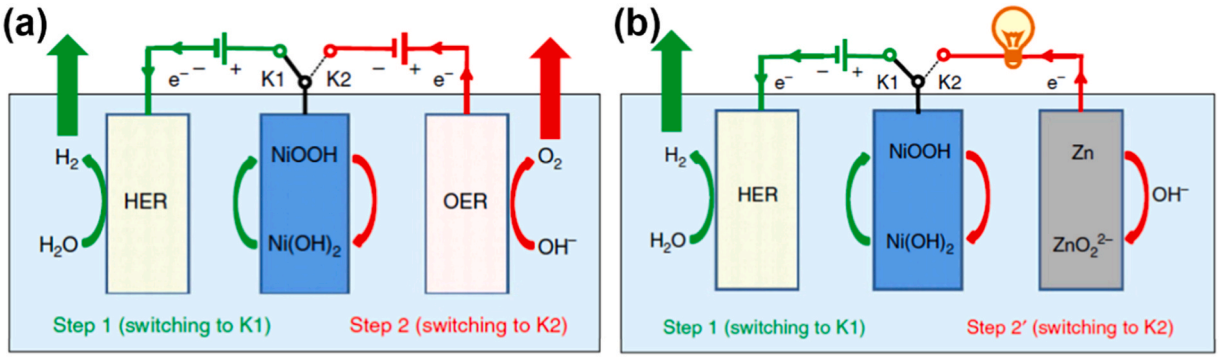

Fig. 8. Schematic illustration of $Ni(OH)_2$ as solid redox electrode for separation of (a) HER and OER in water electrolysis and (b) HER and discharge of (−) Zn | 1 mol L^{-1} KOH | NiOOH (+) battery instead of OER [76].

$$Zn + 4OH^- - 2e = ZnO_2^{2-} + 2H_2O \quad (20)$$

Almost simultaneously, the concept of using $Ni(OH)_2$ as the redox electrode was also applied in the separation of HER and OER [77]. As we know, a salt bridge, which can separate the anodic and cathodic reactions in two compartments, is not a practical operation, because the series resistance of a salt bridge reduces the electrolysis efficiency. That is why a PEM or AEM was used to separate the anode and cathode compartments. Drawing a lesson from the configuration of the salt bridge, the design of the separated water electrolysis by two electrically connected $Ni(OH)_2$/NiOOH redox electrodes in Fig. 9a realised that HER and OER occurred simultaneously in different spaces. The $Ni(OH)_2$ electrode paired with the HER electrode whilst the NiOOH electrode with OER. The electrolysis curves of the system delivered an average voltage of 2.12 V. In order to avoid the OER (or HER) side reaction in the HER (or OER) compartment, threshold values were set. It is worth noting that the electrolysis curves ended with a sudden jump, indicative of complete charging and discharging of the redox electrodes. However, when the charging capacity exceeded 80%, the opposite side reactions occurred, leading to the mixture of H_2 and O_2. Combining with analysis in the literature with similar jump tails [69], the sudden jump may be associated with the opposite side reactions. The cycle duration decreased by an average of 0.3% per cycle due to polarization or degradation of the redox $Ni(OH)_2$ electrodes. The authors stated that the average voltage drop between the two electrically connected $Ni(OH)_2$ and NiOOH electrodes was 0.12 V, but from the corresponding figure in the literature [77], at least 0.38 V of voltage drop can be seen. The authors stated that the energy efficiency was 58% by comparing with the theoretical 1.23 V, for which only HER was considered. Perhaps as the energy efficiency was low, a hydrogen fuelling station with unsealed PEC solar cells or photoelectrochemical-photovoltaic (PEC-PV) tandem cells was envisaged. For a hydrogen fuelling station with a production rate of 400 kg H_2 per day, an array consisting of >3000000 cells was required under a series of reasonable assumptions. The configuration of the PEC-PV system is shown in Fig. 9b, in which a Si PV module was conformally mapped by the OER electrode connected to the Ni foil and the Pt coated mesh electrodes in the OER and HER cells, respectively. The polarization curves of the PV module and the two-cell PEC system crossed at 1.7 V and 6.7 mA cm^{-2}. However, the coupled PEC-PV system was operated at slightly higher voltages and lower current densities due to additional coupling losses such as contact resistances. Finally, the solar to energy efficiency of 7.5% was obtained.

As referenced in literature [77], the metal Ni anodes in the PEC-PV system could be replaced by semiconductor photoanodes, such as hematite (α-Fe_2O_3). Scalable PEC-PV tandem devices were proposed, wherein the oxygen cell contained two 100 cm^2 back-to-back hematite photoanodes placed in tandem with Si PV mini-modules [78]. For a hydrogen fuelling station, the HER and OER cells are fixed. Hence, after the $Ni(OH)_2$ electrode in the HER cell was charged and the NiOOH electrode in the OER cell discharged, the two redox electrodes must be swapped between the cells to continue operating. A swapping scheme was designed consisting of intracell swapping in the OER cell with the more complicated structure of photoanode/PV stack and subsequent intercell swapping between OER and HER cells. Furthermore, full charge and discharge should be strictly avoided due to competitive side reactions of OER and HER. The state of charge (SOC) or discharge could not exceed 28% in practical applications. Incomplete charging of the $Ni(OH)_2$ electrode in the HER cell would lead to operational instability due to charge accumulation. This has to be amended by discharging the electrodes to their initial state between cycles. Accordingly, between cycles, the HER cell was disconnected from the OER cell and the two cells operated separately at a constant voltage of 1.45 V for an additional 45 mAh for drift-free water splitting cycles. The extra step is too complicated to make the method based on the $Ni(OH)_2$ redox electrodes unrealistic in practical applications.

Cobalt substitution can shift the $Ni(OH)_2$/NiOOH redox potential negatively, suppressing the side reaction of OER when charging the $Ni(OH)_2$ electrodes in the decoupled water electrolysis. Therefore, $Ni_{0.9}Co_{0.1}(OH)_2$ anodes can be charged to a higher SOC without competitive OER. The authors stated that the sharp current peak in CV was from pseudocapacitive $Ni_{0.9}Co_{0.1}(OH)_2$ anode oxidation [79], which confuses the concepts of battery and pseudocapacitive behaviours [80]. In the first step, when $Ni(OH)_2$ in $Ni_{0.9}Co_{0.1}(OH)_2$ was oxidised to NiOOH, concurrent HER occurred at 25 °C. It was found that the $Ni(OH)_2$ electrode regenerated from NiOOH with spontaneous OER in a hot electrolyte at 95 °C in the second step. The swinging of the cold and hot electrolyte realised the continuous alternate water splitting, during which the hot loss should be controlled by heat management.

The FeP-CoP/N doping carbon bifunctional catalysts were applied in the alternate water electrolysis with the redox $Ni(OH)_2$ and NiOOH electrodes in the flow electrolytes [81]. The cell voltages of HER and OER lasting for 10 min each cycle were 2.1 and −2.1 V at a high current density of 750 mA cm^{-2}.

4.2. Organics

Recently, organic lithium-ion batteries have been gaining prominence. The corresponding electrode materials rely solely on naturally abundant elements such as carbon, hydrogen, nitrogen and oxygen rather than the rare and expensive elements like lithium and cobalt. These lighter elements means that organic batteries have greater theoretical capacities compared with conventional lithium-ion batteries, albeit with lower specific energies due to their relatively low working voltage [82,83]. Polytriphenylamine (PTPAn) previously utilised as the electrode material in organic lithium-ion batteries, can also serve as a solid state redox mediator to separate HER and OER in water electrolysis [84]. The capacity of PTPAn delivered a reversible capacity of 77 mAh g^{-1} in 0.5 mol L^{-1} H_2SO_4 at 0.2 A g^{-1}, which was much higher than the theoretical capacity of 18.6 mAh g^{-1} for the soluble ECPB of

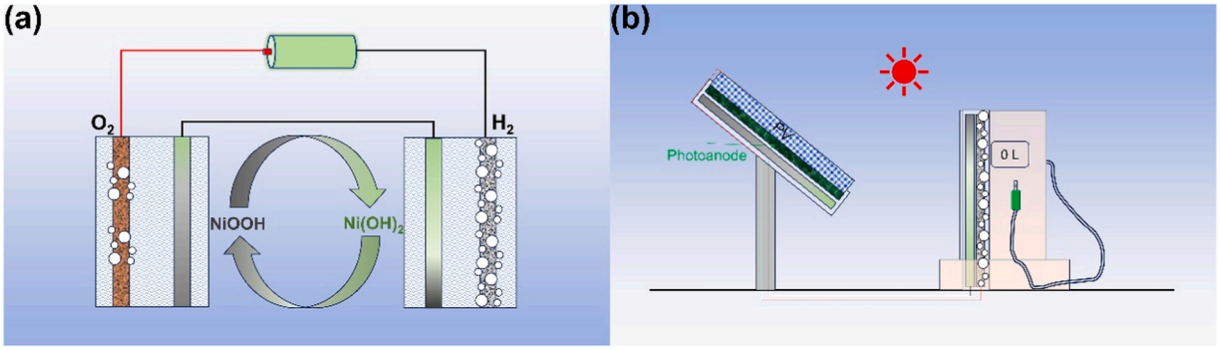

Fig. 9. Schematic illustration of electrically connected $Ni(OH)_2$ and NiOOH as solid redox electrodes for separation of HER and OER in different spaces (a) in water electrolysis and (b) PEC-PV system [77].

silicotungstic acid. If H_2SO_4 electrolyte as an electrolyte, the anodic n-type doping of PTPAn along with HER in the first step are described in Eq. (21).

$$PTPAn + SO_4^{2-} - 2e = PTPAn^{2+}||SO_4^{2-} \quad (21)$$

The reverse reaction of Eq. (21) evoked OER in the second step. Finally, decoupled water electrolysis was driven by a PV cell. The solar to hydrogen efficiency was 5.4%.

A similar research was that pyrene-4,5,9,10-tetraone (PTO) as a solid-state proton buffer electrode with a larger specific capacity to separate HER and OER [85].

4.3. $Na_{0.44}MnO_2$ for chlor-alkali process

The chlor-alkali process was virtually electrolysis of saline solution. As the $Na_{0.44}MnO_2$ is the electrode of sodium-ion batteries, it was also used as the redox electrode to alternate HER and ClER in the chlor-alkali process [86]. The mechanism of the redox $Na_{0.44}MnO_2$ electrode involved the deintercalation and intercalation of Na ions from and to $Na_{0.44}MnO_2$. As OH^- ions were produced during HER, the corresponding electrolyte was 1 mol L^{-1} NaOH, whilst the electrolyte in the ClER step was a saturated NaCl solution. The redox electrode had to be washed by new electrolyte and moved to the cell in the next step. The ClER faradaic efficiency was 90.2% in the two-step process, which was slightly smaller than 97.4% in the conventional chlor-alkali process.

If HER is not as crucial in the chlor-alkali process, an ORR electrode with an electrolytic MnO_2 catalyst can replace the HER electrode to lower the electrolysis voltage. On the other hand, to prevent $Na_{0.44}MnO_2$ from the causticity of chlorates, the $Na_{0.44}MnO_2$ and Ag/AgCl redox electrodes divided the chlor-alkali process into three steps. The first step involved ORR and the oxidation of $Na_{0.44}MnO_2$ and the third step was reduction of AgCl to Ag and ClER. The second step between them is essentially a battery course rather than electrolysis, in which $Na_{0.44-x}MnO_2$ and Ag act at positive and negative electrodes [87]. The process was overly complicated and seemed to have little relevance to water electrolysis. Certainly, $Na_{0.44-x}MnO_2$ is no problem in achieving alternate water electrolysis with decoupled HER and OER [88].

4.4. Others

In addition to $Ni(OH)_2$, $NaMnO_2$ and organics as redox electrodes, other some redox electrodes were also used, such as the $(Ni_5Mn)_2P$ on nickel foams [89], CuO/Cu_2O [90], polyaniline [91] and $NaTi_2(PO_4)_3$ [92] electrodes. The former two works stated that the materials showed the pseudocapacitive behaviours which in fact were Nerst characteristic peaks in CVs. In the latter work [92], $Ni(OH)_2$ was also investigated in alternate water electrolysis along with a trifunctional electrode of Ni_3S_2/CNT foam which acted as a catalyst for HER, ORR and OER. In the first step, NiOOH was reduced to $Ni(OH)_2$, accompanying concurrent OER. In the second step, when $Ni(OH)_2$ was oxidised to NiOOH, ORR, which has a potential higher than HER on Ni_3S_2, occurred firstly if residual O_2 was trapped on the catalytic electrode or dissolved in the electrolyte, subsequently HER occurred. It was asserted that the ORR course could consume the residual O_2 after OER. However, it was also inevitable to consume the charging capacity of $Ni(OH)_2$ and hence reduced the amount of produced H_2 in the second step.

5. Alternate half-electrolysis of water

5.1. Half-electrolysis

In 2014, the concept of half-electrolysis was proposed to reduce the energy consumption of conventional electrolysis [93]. In conventional electrolysis, there are two faradaic redox half-reactions. Half-electrolysis was defined to run only one wanted faradaic redox half-reaction for electrolysis with the aid of a supercapacitor electrode. The charge storage of the supercapacitor electrode relies on a non-faradaic electric double layer (EDL). Therefore, the other unwanted counter electrode reaction is eliminated in the half-electrolysis process. As a result, the whole electrolysis voltage as well as the electrical energy consumption, part of which is supposed to be afforded on the unwanted counter electrode, is remarkably reduced. Typically, polypyrrole can be synthesized by electric polymerization by anodic electrolysis. In conventional electrolysis, HER in the cathode concurrently occurred with the oxidation of pyrrole monomer in the anode. The oxidation of pyrrole is wanted but the energy consumed by HER is unwanted for the production of polypyrrole by electrolysis. The onset potential of pyrrole polymerization and HER in the electrolyte containing pyrrole and KCl with Ti electrodes was 0.68 V and −1.3 V, respectively, indicating that the conventional electrolysis voltage is at least 1.98 V. The conventional cell required 2.00 V to drive the electrolysis in CV (Fig. 10a), which highly agreed with the potential difference between the onset potential of pyrrole polymerization and HER. To avoid a large amount of electrical energy being wasted in HER, an EDL electrode of commercial activated carbon (CMPB) replaced the previous Ti cathode. The half-electrolysis cell only required 0.55 V to drive the pyrrole polymerization. In galvanostatic electrolysis (Fig. 10b), the conventional electrolysis delivered a nearly constant voltage of 2.15 V. The half-electrolysis cell exhibited a much lower initial voltage of 0.586 V, which was attributed to the low open circuit potential of CMPB. The voltage increased with electrolysis time because the potential of the CMPB electrode shifted to more negative values. According to Eq. (22), the energy consumption of the half-electrolysis accounted for 81.4% of that of the conventional electrolysis, meaning that the half-electrolysis could save 18.6% of the electric energy.

$$W = I\int_0^t Udt \quad (22)$$

5.2. Half-electrolysis of water

However, the challenge with half-electrolysis lies in how to easily continue the process once the supercapacitor electrode is fully charged. Relying on the self-discharge of the supercapacitor electrode, though partially feasible [93], is not a comprehensive method to regenerate the supercapacitor electrode for sustaining the half-electrolysis. If half-electrolysis is applied to water electrolysis, it would work continuously to achieve alternate water electrolysis, as revealed in our patent applications in 2019 [94,95]. Typically, the cell for the half-electrolysis of water consisted of a supercapacitor electrode of activated carbon (AC), an electrolysis electrode of commercial Pt wire or Pt/C in an electrolyte of simulated seawater with an alkaline additive (0.5 mol L^{-1} KOH + 0.5 mol L^{-1} NaCl). When the AC electrode was charged, HER occurred on the Pt electrode as a cathode according to Eq. (17), whilst AC discharged, OER on the same Pt electrode as an anode according to Eq. (19) [96]. Because HER and OER occurred stepwise, the diaphragm was omitted in the half-electrolysis of water, overcoming the drawbacks of a diaphragm-based cell mentioned in Introduction.

It is crucial to note that the half-electrolysis of water differs essentially from decoupling HER and OER with redox solid electrodes by faradaic reactions in last session, because only one faradaic reaction, for example either Eq. (17) for HER or Eq. (19) for OER, occurred during each step in the half-electrolysis of water, rather than two faradaic reactions, for example Eqs. (16) and (17) for HER or Eqs. (18) and (19) for OER. The AC electrode, different from those materials with Nerst CV peaks, stores electric energy by a highly reversible EDL mechanism and hence help realize the real “half-electrolysis”, which is expected to increase the applied current and prolong the lifetime of the instrument. It is important to emphasize again that the sharp Nerst characteristic current peaks in CV are arising from faradaic reactions having fixed redox potentials rather than pseudocapacitive behaviours, similar to

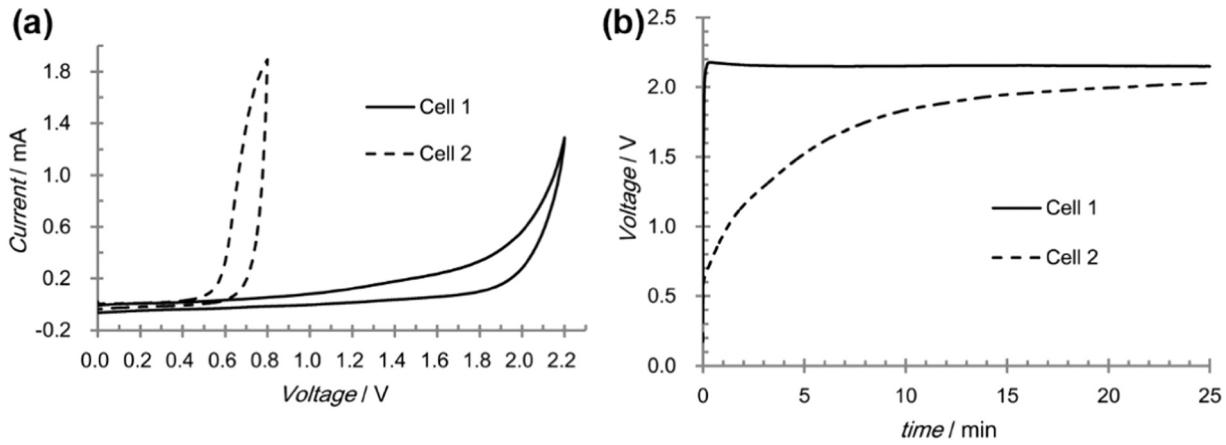

Fig. 10. (a) CVs and (b) galvanostatic electrolysis of Cell 1 (conventional) and Cell 2 (half-electrolysis) [93].

EDL mechanisms, having no peaks in CV [80]. A work on decoupling HER and OER even confused the AC electrode with redox medium [88].

The key of the half-electrolysis of water is the energy comparison with conventional water electrolysis. Firstly, the half-electrolysis cell was compared with the ideal conventional electrolyser without a diaphragm but with two identical Pt electrodes in alkaline saline water. The conventional cell required a constant voltage of 3.548 V at 50 mA cm^{-2}. Nevertheless, the electrolysis curve of the half-electrolysis cell was superimposed. To produce equal amounts of H_2 and O_2, the energy consumption of the half-electrolysis cell accounted for 96% of the ideal conventional cell (Fig. 11a). Then the conventional electrolyser without and with the diaphragm was investigated. The conventional cell without the diaphragm delivered a nearly constant voltage of 4.459 V, whilst that with a diaphragm 4.943 V, as shown in Fig. 11b, indicating a diaphragm resistance of 7.563 Ω. The increased energy consumption by 10% resulted from the diaphragm. Comparing with the conventional cell with the diaphragm, the half-electrolysis of water saved 14% in energy input. The same 14% energy saved was realised at 20.0 mA cm^{-2}. When the electrolyte was changed to 1 mol L^{-1} Na_2SO_4, a PEM with high electric conductivity replaced the diaphragm in the conventional electrolysis. Finally, the half-electrolysis also saved 8% of energy input compared with the PEM based electrolyser.

With the aid of the supercapacitor electrode, the half-electrolysis of water could independently adjust the cathodic and anodic currents and last for 300 cycles, equivalent to 123 h in the Na_2SO_4 electrolyte. Similar excellent cyclic performance is observed in acidic and alkaline saline water electrolytes. Furthermore, no Cl_2 was detected during cycling in the alkaline saline water electrolytes. However, the faradaic efficiency of OER with the commercial Pt wire electrode was only 65.2%. The *N*,*N*-diethyl-p-phenylenediamine (DPD) method indicated that competitive hypochlorite was produced, resulting in the low OER efficiency. When Pt/C replaced the Pt wire, after HER and OER each for 700 s, the corresponding volumes of H_2 and O_2 were 5.6 and 2.75 mL, corresponding to 98.0% and 96.3% in current efficiency, respectively (Fig. 12). The faradaic efficiency of OER increased to nearly 100% due to a higher active surface area in Pt/C impeding hypochlorite formation.

5.3. Advantages of half-electrolysis

Evidently, due to the supercapacitor electrode based on the EDL mechanism, the half-electrolysis of water offers several advantages compared with alternate water electrolysis with liquid and solid redox mediums. Firstly, the half-electrolysis of water is expected to afford a larger electrolysis current than other systems with redox mediums due to the high electric conductivity of the supercapacitor electrode. The high electric conductivity also enhances the utilization rate of active electrode materials. Typically, $Ni(OH)_2$, a redox solid electrode, requires the introduction of CNTs for high electric conductivity, leading to a decrease in active content to 60% [76]. However, if a graphene membrane with high electric conductivity is used, the active component

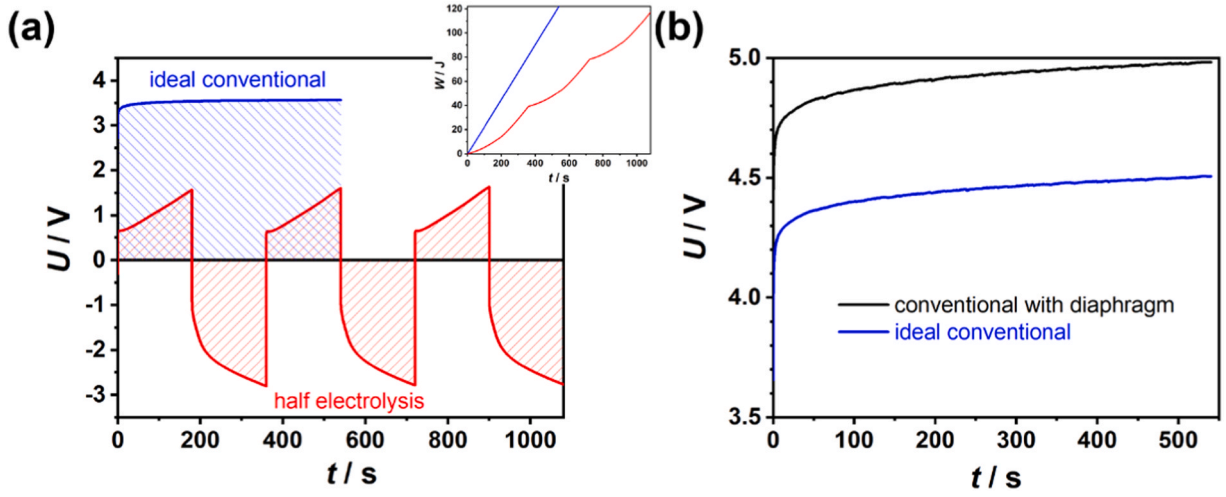

Fig. 11. Galvanostatic electrolysis comparison between (a) half-electrolysis and ideal conventional electrolysis without diaphragm as well as energy comparison in inset of (a), (b) conventional cell with two identical Pt wire electrodes with or without diaphragm at 50.0 mA cm^{-2} in alkaline saline water electrolyte [96].

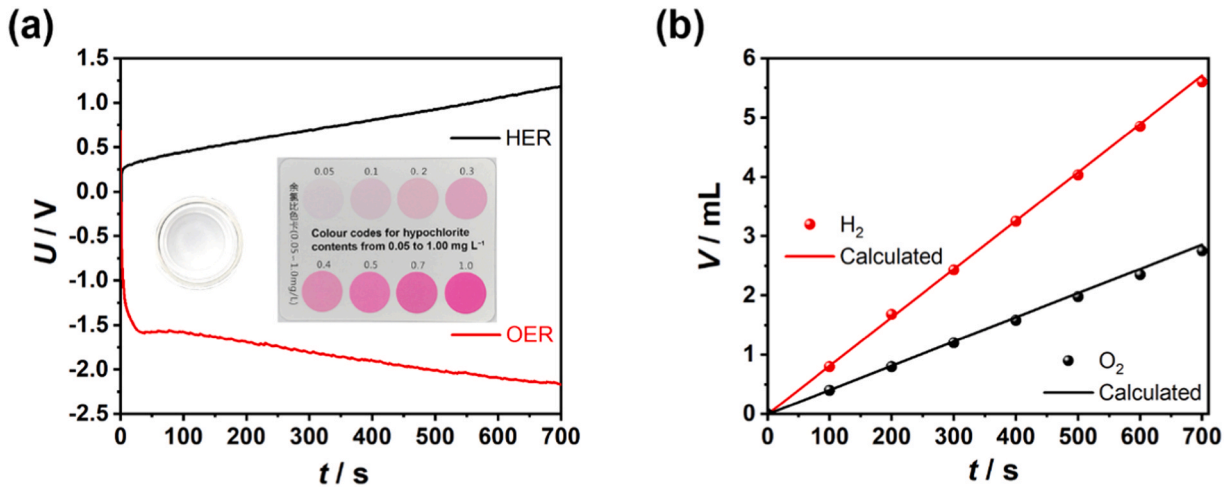

Fig. 12. (a) Galvanostatic electrolysis curves of half-electrolysis of alkaline saline water consisting of the AC electrode of 54.1 F and Pt/C pasted on the Pt wire electrode at 50 mA cm^{-2} with inset of (a) DPD method after electrolysis. (b) Volumes of H_2 (red dots) and O_2 (black dots) collected with burette (markers) at different times and calculated (lines) from the charge passed during electrolysis [96].

content can reach 100%. Secondly, the supercapacitor electrode with high reversibility and coulombic efficiency can results in better cyclic performance than alternate water electrolysis with redox mediums with faradaic reactions. Thirdly, supercapacitor electrodes can adapt to acidic, neutral, alkaline and even seawater with different pH values. In contrast, liquid redox mediums of polyoxometallic acids or solid redox mediums like $Ni(OH)_2$ can only be applied in acidic or alkaline electrolytes. Fourthly, supercapacitor electrodes can fully utilize the potential range between HER and OER. Not all polyoxometallic acids have redox potentials within the potential range between HER and OER, especially when Pt electrodes are applied. For example, the more negative reduced peak of the $H_4[SiW_{12}O_{40}]$ solution is beyond potentials of HER with the Pt electrode [42]. As the potential of all supercapacitor electrodes must be within the range between HER and OER in the corresponding electrolyte, all supercapacitor electrodes can realize the alternate half-electrolysis of water. Of course, the same applies to the redox electrodes in aqueous batteries. The potential range change of the supercapacitor electrode can reach at least 1 V which is 100% of SOC, however, SOC of $Ni(OH)_2$ cannot exceed 28% in practical applications [78]. Last but not least, it is demonstrated for the first time that the half-electrolysis of water can save 14% of energy input, corresponding to 86% of the energy ratio of alternate water electrolysis to practical conventional with membrane or diaphragm, as shown in Table 1. Other literature on whether liquid [41,42] or solid [76] redox mediums showed that the energy ratios were beyond 100%, meaning that their systems of alternate water electrolysis consume more energy than those of conventional water electrolysis.

6. Conclusions and perspective

The main challenges of conventional water electrolysis include the explosive mixture of hydrogen and oxygen gases and high energy consumption. To address these issues, alternate water electrolysis has been developed by decoupling HER and OER.

Solar water thermolysis with decoupled H_2 and O_2 production can be achieved via multistep thermochemical processes with metal oxides as redox mediums at temperatures much lower than that for one-step water thermolysis. The main issue is that the metal formed from reduction of the metal oxide can be readily passivated and retard H_2 production. Electrolysis replacing thermochemistry in HER could overcome passivation when metal is oxidised to metal oxide but exhibited low efficiency. Using redox couples of low valence metal oxide/high valence metal oxide could increase the cycle efficiency to above 60%. The electrolysis for HER only requires 0.7 V when the Fe_3O_4 particles are used as the anode. It is demonstrated that the proposed concept of alternate thermolysis and electrolysis of water with a metal oxide anode is possibly feasible in industry.

Alternate water electrolysis can be realised by the liquid redox mediums at room temperature. Polyoxometallic acids, such as $H_3PMo_{12}O_{40}$ and $H_4SiW_{12}O_{40}$, can be used as an electron-coupled proton buffer (ECPB) to decouple HER and OER. The spontaneous HER on the reduced $H_4SiW_{12}O_{40}$ can separate HER and OER in space, further preventing the mixing of H_2 and O_2. The exploitation of a multi-electron ECPB can decrease the cycle times. Between neighbouring cycles, the extra purge has to be done in the same electrolysis time. Small organic molecules can also be used as the ECPB but the degradation is more severe. The long

Table 1
Comparison of half electrolysis of water with other alternate water electrolysis with redox mediums.

Medium	OER electrode	J[a] / mA cm^{-2}	t / h (cycle)[a]	pH	SOC / %	η_{HER} / %	η_{OER} / %	E_a/E_{ic}[b] / %	E_a/E_{pc}[c] / %	Ref.
AC	Pt wire	195	123 (300)	0–14	100	97.0	65.2	96	86	[96]
	Pt/C					98.0	96.3			
$H_3PMo_{12}O_{40}$	Pt disk	>250	4.4 (500)	0.3	—	100	100	—	127	[41]
$H_4SiW_{12}O_{40}$	Pt	130	200 (20)	0.5	60	68	100	—	107[d]	[42]
$Ni(OH)_2$	RuO_2/IrO_2	100	6.7 (20)	14	—	94.7	94.7	109	—	[76]
$Ni(OH)_2$	Ni	5	20 (20)	14	80	100	100	—[e]	—	[77]
$Ni(OH)_2$	Fe_2O_3	0.55	82 (10)	14	28	100	100	—	—	[78]

[a] Maximum value in paper.
[b] Energy consumption ratio of alternate water electrolysis to ideal conventional without membrane, <100 means saving energy.
[c] Energy consumption ratio of alternate water electrolysis to practical conventional with membrane, <100 means saving energy.
[d] 107% not consider low faradaic efficiency of spontaneous HER.
[e] calculation in paper cannot be compared.

run time for each cycle is the advantage of the alternate water electrolysis with the liquid redox mediums. However, in the alternate water electrolysis by the liquid redox mediums, the membrane, even more than one, is still inevitable and the energy consumptions are readily increased in comparison with the conventional water electrolysis, especially considering the practical situation such as the increased flow rate.

Alternate water electrolysis can also be realised by the solid redox mediums, typically such as $Ni(OH)_2$ and $Na_{0.44}MnO_2$. In these systems, omitted membranes and usage of alkaline electrolytes can save the cost of the instrument. For the sake of electric conductivity, CNTs may be introduced, resulting in the low utilisation of $Ni(OH)_2$. The energy consumption of the alternate water electrolysis with the solid redox medium is slightly higher than that of the ideal conventional water electrolysis without membrane. If building the scalable solar driven hydrogen fuelling station, only 28% of SOC of $Ni(OH)_2$ can be utilised. Solid organic redox electrodes can also execute the alternate water electrolysis.

Alternate half-electrolysis of water relies on a supercapacitor electrode based on the EDL mechanism to realise the stepwise HER and OER. The membrane or diaphragm can also be omitted. The half-electrolysis of water is supposed to afford a larger electrolysis current and a longer cyclic performance. The half-electrolysis system can adopt to various aqueous electrolytes with different pH values. Nearly 100% SOC of the supercapacitor electrode can be utilised. The most important is that the energy consumption of the half-electrolysis of water can be saved by 14% and 8%, comparing with the practical conventional water electrolysis with a diaphragm and PEM, respectively.

Liquid redox mediums cannot help the alternate water electrolysis omit the expensive membranes. So far, the alternate water electrolysis by the liquid redox mediums cannot replace the conventional water electrolysis in terms of instrument cost and energy saving. Even if using the spontaneous HER, the faradaic efficiency is also low. The spontaneous HER is virtually a chemical catalysis process and hence it cannot replace the chemical catalysis to produce H_2 from some hydrogen storage materials with lighter weights, such as formic acid and ammonia borane. The alternate water electrolysis with the solid redox mediums can eliminate the membranes, but the energy consumption is still slightly larger than that of the conventional water electrolysis.

The alternate half-electrolysis of water has the advantages of membrane free and energy saving, compared with the other two systems of alternate water electrolysis. The energy consumption can be saved by the alternate half-electrolysis of water due to the highly reversible supercapacitor electrode without redox reactions. Therefore, among all alternate water electrolysis systems, the half-electrolysis of water is the most promising in the future industrial application. However, the half-electrolysis of water based on the supercapacitor electrode confronts some challenges. The main challenge arises from the supercapacitor electrode. Compared with the liquid and even solid redox mediums, the supercapacitor electrodes have much smaller specific charge capacity, which means the number of cycles in the half-electrolysis of water must increase in the same electrolysis time, meaning that more frequent purge between cycles might be necessary. On the one hand, the specific capacitance of carbon materials should be improved. The reversible pseudocapacitive materials, such as RuO_2 which show the rectangular CVs without current peaks, incorporated into carbon materials should be investigated. On the other hand, the elegant configuration of half-electrolysis of water should be designed. Multiple supercapacitor electrodes could be designed to surround the catalyst electrode. The whole half-electrolysis of water could be designed to separate HER and OER in space as well. Even the half-electrolysis instrument could combine the supercapacitors to circulate the HER courses. The other challenges of the half-electrolysis of water include the development of seawater-based electrolytes [97], more efficient and affordable catalysts [98], and design and manufacture of the whole instrument.

It is worth noting that the innovative strategy of hybrid water electrolysis which employ thermodynamically favourable oxidation reaction to replace OER can also realise the energy-saving hydrogen generation plus value-added chemicals [99–103]. The supplemental solution to address the issues in conventional water electrolysis can be also applied in the alternate water electrolysis. With the unremitting efforts from multidiscipline researchers, it is believed that the alternate water electrolysis can open up a significant vista for hydrogen generation in the near future.

Declaration of Competing Interest

The authors declare that they have no known competing financial interests or personal relationships that could have appeared to influence the work reported in this paper.

Acknowledgments

Y. Chen gratefully acknowledges the financial support from the National Natural Science Foundation of China (21905216). G. Z. Chen thanks EPSRC (EP/J000582/1 and GR/R68078) and Innovate UK (Smart grants, 10017140).

References

[1] K. Uddin, Nuclear energy, environment and public safety: North-south politics, Strateg. Plan. Energy Environ. 38 (2019) 31–41, https://doi.org/10.1080/10485236.2019.12054410.
[2] D.J. Durbin, C. Malardier-Jugroot, Review of hydrogen storage techniques for on board vehicle applications, Int. J. Hydrog. Energy 38 (2013) 14595–14617, https://doi.org/10.1016/j.ijhydene.2013.07.058.
[3] P.J. Megía, A.J. Vizcaíno, J.A. Calles, A. Carrero, Hydrogen production technologies: from fossil fuels toward renewable sources. A mini review, Energy Fuels 35 (2021) 16403–16415, https://doi.org/10.1021/acs.energyfuels.1c02501.
[4] I. Roger, M.A. Shipman, M.D. Symes, Earth-abundant catalysts for electrochemical and photoelectrochemical water splitting, Nat. Rev. Chem. 1 (2017) 0003, https://doi.org/10.1038/s41570-016-0003.
[5] R.M. Navarro, R. Guil, J.L.G. Fierro, 2 - Introduction to hydrogen production, in: V. Subramani, A. Basile, T.N. Veziroğlu (Eds.), Compendium of Hydrogen Energy, Woodhead Publishing, Oxford, 2015, pp. 21–61.
[6] S. Trasatti, Water electrolysis: who first? J. Electroanal. Chem. 476 (1999) 90–91, https://doi.org/10.1016/S0022-0728(99)00364-2.
[7] T. Smolinka, H. Bergmann, J. Garche, M. Kusnezoff, Chapter 4 - The history of water electrolysis from its beginnings to the present, in: T. Smolinka, J. Garche (Eds.), Electrochemical Power Sources: Fundamentals, Systems, and Applications, Elsevier, 2022, pp. 83–164.
[8] G.Z. Chen, Supercapacitor and supercapattery as emerging electrochemical energy stores, Inter. Mater. Rev. 62 (2017) 173–202, https://doi.org/10.1080/09506608.2016.1240914.
[9] X. Xu, Z. Shao, S.P. Jiang, High-entropy materials for water electrolysis, Energy Technol. 10 (2022), https://doi.org/10.1002/ente.202200573.
[10] S. Dresp, F. Dionigi, M. Klingenhof, P. Strasser, Direct electrolytic splitting of seawater: Opportunities and challenges, ACS Energy Lett. 4 (2019) 933–942, https://doi.org/10.1021/acsenergylett.9b00220.
[11] M. Chatenet, B.G. Pollet, D.R. Dekel, F. Dionigi, J. Deseure, P. Millet, R.D. Braatz, M.Z. Bazant, M. Eikerling, I. Staffell, P. Balcombe, Y. Shao-Horn, H. Schäfer, Water electrolysis: From textbook knowledge to the latest scientific strategies and industrial developments, Chem. Soc. Rev. 51 (2022) 4583–4762, https://doi.org/10.1039/D0CS01079K.
[12] S.A. Grigoriev, V.N. Fateev, D.G. Bessarabov, P. Millet, Current status, research trends, and challenges in water electrolysis science and technology, Int. J. Hydrog. Energy 45 (2020) 26036–26058, https://doi.org/10.1016/j.ijhydene.2020.03.109.
[13] M. Yu, E. Budiyanto, H. Tuysuz, Principles of water electrolysis and recent progress in cobalt-, nickel-, and iron-based oxides for the oxygen evolution reaction, Angew. Chem. Int. Ed. 61 (2022), https://doi.org/10.1002/anie.202103824.
[14] H. Wu, Y. Wang, Z. Shi, X. Wang, J. Yang, M. Xiao, J. Ge, W. Xing, C. Liu, Recent developments of iridium-based catalysts for the oxygen evolution reaction in acidic water electrolysis, J. Mater. Chem. A 10 (2022) 13170–13189, https://doi.org/10.1039/D1TA10324E.
[15] J. Yang, M.J. Jang, X. Zeng, Y.S. Park, J. Lee, S.M. Choi, Y. Yin, Non-precious electrocatalysts for oxygen evolution reaction in anion exchange membrane water electrolysis: a mini review, Electrochem. Commun. 131 (2021) 107118, https://doi.org/10.1016/j.elecom.2021.107118.
[16] S. Wang, A. Lu, C.-J. Zhong, Hydrogen production from water electrolysis: role of catalysts, Nano Converg. 8 (2021) 4, https://doi.org/10.1186/s40580-021-00254-x.

[17] C. Jo, S. Surendran, M.-C. Kim, T.-Y. An, Y. Lim, H. Choi, G. Janani, S. Cyril Jesudass, D. Jun Moon, J. Kim, J. Young Kim, C. Hyuck Choi, M. Kim, J. Kyu Kim, U. Sim, Meticulous integration of N and C active sites in Ni_2P electrocatalyst for sustainable ammonia oxidation and efficient hydrogen production, Chem. Eng. J. 463 (2023) 142314, https://doi.org/10.1016/j.cej.2023.142314.

[18] Y. Chen, Z. Xu, G.Z. Chen, Nano-scale engineering of heterojunction for alkaline water electrolysis, Materials 17 (2024) 199.

[19] W. Tong, M. Forster, F. Dionigi, S. Dresp, R. Sadeghi Erami, P. Strasser, A. J. Cowan, P. Farràs, Electrolysis of low-grade and saline surface water, Nat. Energy 5 (2020) 367–377, https://doi.org/10.1038/s41560-020-0550-8.

[20] J. Chi, H. Yu, Water electrolysis based on renewable energy for hydrogen production, Chin. J. Catal. 39 (2018) 390–394, https://doi.org/10.1016/S1872-2067(17)62949-8.

[21] J. Yang, J. Li, B. Liu, D. Yan, L. Jia, X. Han, K. Wu, J. Li, High and durable performance of an external-manifold designed reversible solid oxide cell stack, J. Power Sources 580 (2023) 233390, https://doi.org/10.1016/j.jpowsour.2023.233390.

[22] Y. Zheng, S.-Z. Qiao, Direct seawater splitting to hydrogen by a membrane electrolyzer, Joule 7 (2023) 20–22, https://doi.org/10.1016/j.joule.2022.12.017.

[23] J.N. Hausmann, R. Schlögl, P.W. Menezes, M. Driess, Is direct seawater splitting economically meaningful? Energy Environ. Sci. 14 (2021) 3679–3685, https://doi.org/10.1039/D0EE03659E.

[24] P. Farràs, P. Strasser, A.J. Cowan, Water electrolysis: direct from the sea or not to be? Joule 5 (2021) 1921–1923, https://doi.org/10.1016/j.joule.2021.07.014.

[25] A.G. Wallace, M.D. Symes, Decoupling strategies in electrochemical water splitting and beyond, Joule 2 (2018) 1390–1395, https://doi.org/10.1016/j.joule.2018.06.011.

[26] J. Huang, Y. Wang, Efficient renewable-to-hydrogen conversion via decoupled electrochemical water splitting, Cell Rep. Phys. Sci. 1 (2020), https://doi.org/10.1016/j.xcrp.2020.100138.

[27] P.J. McHugh, A.D. Stergiou, M.D. Symes, Decoupled electrochemical water splitting: From fundamentals to applications, Adv. Energy Mater. 10 (2020) 2002453, https://doi.org/10.1002/aenm.202002453.

[28] Z.P. Ifkovits, J.M. Evans, M.C. Meier, K.M. Papadantonakis, N.S. Lewis, Decoupled electrochemical water-splitting systems: a review and perspective, Energy Environ. Sci. 14 (2021) 4740–4759, https://doi.org/10.1039/D1EE01226F.

[29] A. Paul, M.D. Symes, Decoupled electrolysis for water splitting, Curr. Opin. Green. Sustain. Chem. 29 (2021) 100453, https://doi.org/10.1016/j.cogsc.2021.100453.

[30] J.E. Lee, I. Shafiq, M. Hussain, S.S. Lam, G.H. Rhee, Y.-K. Park, A review on integrated thermochemical hydrogen production from water, Int. J. Hydrog. Energy 47 (2022) 4346–4356, https://doi.org/10.1016/j.ijhydene.2021.11.065.

[31] J.E. Funk, R.M. Reinstrom, Energy requirements in production of hydrogen from water, Ind. Eng. Chem. Proc. Des. Dev. 5 (1966) 336–342, https://doi.org/10.1021/i260019a025.

[32] R.E. Chao, Thermochemical water decomposition processes, Prod. RD 13 (1974) 94–101, https://doi.org/10.1021/i360050a002.

[33] T. Nakamura, Hydrogen production from water utilizing solar heat at high temperatures, Sol. Energy 19 (1977) 467–475, https://doi.org/10.1016/0038-092X(77)90102-5.

[34] R. Müller, A. Steinfeld, H_2O-splitting thermochemical cycle based on ZnO/Zn-redox: Quenching the effluents from the ZnO dissociation, Chem. Eng. Sci. 63 (2008) 217–227, https://doi.org/10.1016/j.ces.2007.09.034.

[35] M. Comtat, M. Ducarroir, F. Sibieude, G. Crozat, B. Spinner, Theoretical and experimental aspects of a two-step short cycle, based on ZnO and CdO intended for storage of solar energy, Inter. J. Energy Res. 7 (1983) 137–153, https://doi.org/10.1002/er.4440070206.

[36] R. Palumbo, R.B. Diver, C. Larson, E.N. Coker, J.E. Miller, J. Guertin, J. Schoer, M. Meyer, N.P. Siegel, Solar thermal decoupled water electrolysis process I: proof of concept, Chem. Eng. Sci. 84 (2012) 372–380, https://doi.org/10.1016/j.ces.2012.08.023.

[37] S. Nudehi, C. Larson, W. Prusinski, D. Kotfer, J. Otto, E. Beyers, J. Schoer, R. Palumbo, Solar thermal decoupled water electrolysis process II: an extended investigation of the anodic electrochemical reaction, Chem. Eng. Sci. 181 (2018) 159–172, https://doi.org/10.1016/j.ces.2017.12.032.

[38] J.M. Serra, J.F. Borrás-Morell, B. García-Baños, M. Balaguer, P. Plaza-González, J. Santos-Blasco, D. Catalán-Martínez, L. Navarrete, J.M. Catalá-Civera, Hydrogen production via microwave-induced water splitting at low temperature, Nat. Energy 5 (2020) 910–919, https://doi.org/10.1038/s41560-020-00720-6.

[39] J. Barber, Photosynthetic energy conversion: natural and artificial, Chem. Soc. Rev. 38 (2009) 185–196, https://doi.org/10.1039/B802262N.

[40] Y. Wang, H. Suzuki, J. Xie, O. Tomita, D.J. Martin, M. Higashi, D. Kong, R. Abe, J. Tang, Mimicking natural photosynthesis: solar to renewable H_2 fuel synthesis by Z-scheme water splitting systems, Chem. Rev. 118 (2018) 5201–5241, https://doi.org/10.1021/acs.chemrev.7b00286.

[41] M.D. Symes, L. Cronin, Decoupling hydrogen and oxygen evolution during electrolytic water splitting using an electron-coupled-proton buffer, Nat. Chem. 5 (2013) 403–409, https://doi.org/10.1038/nchem.1621.

[42] B. Rausch, M.D. Symes, G. Chisholm, L. Cronin, Decoupled catalytic hydrogen evolution from a molecular metal oxide redox mediator in water splitting, Science 345 (2014) 1326–1330, https://doi.org/10.1126/science.1257443.

[43] Y. Chen, Q.-L. Zhu, N. Tsumori, Q. Xu, Immobilizing highly catalytically active noble metal nanoparticles on reduced graphene oxide: a non-noble metal sacrificial approach, J. Am. Chem. Soc. 137 (2015) 106–109, https://doi.org/10.1021/ja511511q.

[44] Y. Chen, X. Yang, M. Kitta, Q. Xu, Monodispersed Pt nanoparticles on reduced graphene oxide by a non-noble metal sacrificial approach for hydrolytic dehydrogenation of ammonia borane, Nano Res. 10 (2017) 3811–3816, https://doi.org/10.1007/s12274-017-1593-4.

[45] J. Xu, G. Liu, J. Li, X. Wang, The electrocatalytic properties of an IrO_2/SnO_2 catalyst using SnO_2 as a support and an assisting reagent for the oxygen evolution reaction, Electrochim. Acta 59 (2012) 105–112, https://doi.org/10.1016/j.electacta.2011.10.044.

[46] W. Wu, X.-Y. Wu, S.-S. Wang, C.-Z. Lu, Catalytic hydrogen evolution and semihydrogenation of organic compounds using silicotungstic acid as an electron-coupled-proton buffer in water-organic solvent mixtures, J. Catal. 378 (2019) 376–381, https://doi.org/10.1016/j.jcat.2019.09.011.

[47] G. Kear, A.A. Shah, F.C. Walsh, Development of the all-vanadium redox flow battery for energy storage: a review of technological, financial and policy aspects, Inter. J. Energy Res. 36 (2012) 1105–1120, https://doi.org/10.1002/er.1863.

[48] V. Amstutz, K.E. Toghill, F. Powlesland, H. Vrubel, C. Comninellis, X. Hu, H. H. Girault, Renewable hydrogen generation from a dual-circuit redox flow battery, Energy Environ. Sci. 7 (2014) 2350–2358, https://doi.org/10.1039/C4EE00098F.

[49] V.A. Grigoriev, D. Cheng, C.L. Hill, I.A. Weinstock, Role of alkali metal cation size in the energy and rate of electron transfer to solvent-separated 1:1 [(M+)(acceptor)] ($M+ = Li^+$, Na^+, K^+) ion pairs, J. Am. Chem. Soc. 123 (2001) 5292–5307, https://doi.org/10.1021/ja010074q.

[50] H.D. Pratt, N.S. Hudak, X. Fang, T.M. Anderson, A polyoxometalate flow battery, J. Power Sources 236 (2013) 259–264, https://doi.org/10.1016/j.jpowsour.2013.02.056.

[51] J.-J. Chen, M.D. Symes, L. Cronin, Highly reduced and protonated aqueous solutions of $[P_2W_{18}O_{62}]^{6-}$ for on-demand hydrogen generation and energy storage, Nat. Chem. 10 (2018) 1042–1047, https://doi.org/10.1038/s41557-018-0109-5.

[52] G. Chisholm, L. Cronin, M.D. Symes, Decoupled electrolysis using a silicotungstic acid electron-coupled-proton buffer in a proton exchange membrane cell, Electrochim. Acta 331 (2020) 135255, https://doi.org/10.1016/j.electacta.2019.135255.

[53] J. Lei, J.-J. Yang, T. Liu, R.-M. Yuan, D.-R. Deng, M.-S. Zheng, J.-J. Chen, L. Cronin, Q.-F. Dong, Tuning redox active polyoxometalates for efficient electron-coupled proton-buffer-mediated water splitting, Chem. Eur. J. 25 (2019) 11432–11436, https://doi.org/10.1002/chem.201903142.

[54] W. Lubitz, E.J. Reijerse, J. Messinger, Solar water-splitting into H_2 and O_2: design principles of photosystem ii and hydrogenases, Energy Environ. Sci. 1 (2008) 15–31, https://doi.org/10.1039/B808792J.

[55] B. Rausch, M.D. Symes, L. Cronin, A bio-inspired, small molecule electron-coupled-proton buffer for decoupling the half-reactions of electrolytic water splitting, J. Am. Chem. Soc. 135 (2013) 13656–13659, https://doi.org/10.1021/ja4071893.

[56] N. Kirkaldy, G. Chisholm, J.-J. Chen, L. Cronin, A practical, organic-mediated, hybrid electrolyser that decouples hydrogen production at high current densities, Chem. Sci. (2018) 1621–1626.

[57] A. Fujishima, K. Honda, Electrochemical photolysis of water at a semiconductor electrode, Nature 238 (1972) 37–38, https://doi.org/10.1038/238037a0.

[58] Y. Lei, W. Si, Y. Wang, H. Tan, L. Di, L. Wang, J. Liang, F. Hou, Robust carbon nitride homojunction photoelectrode for solar-driven water splitting, ACS Appl. Mater. Interfaces 15 (2023) 6726–6734, https://doi.org/10.1021/acsami.2c18694.

[59] H. Tan, W. Peng, T. Zhang, Y. Han, L. Yin, W. Si, J. Liang, F. Hou, Highly polymerized wine-red carbon nitride to enhance photoelectrochemical water splitting performance of hematite, J. Phys. Chem. C 125 (2021) 13273–13282, https://doi.org/10.1021/acs.jpcc.1c02342.

[60] L.G. Bloor, R. Solarska, K. Bienkowski, P.J. Kulesza, J. Augustynski, M.D. Symes, L. Cronin, Solar-driven water oxidation and decoupled hydrogen production mediated by an electron-coupled-proton buffer, J. Am. Chem. Soc. 138 (2016) 6707–6710, https://doi.org/10.1021/jacs.6b03187.

[61] A. Kudo, K. Ueda, H. Kato, I. Mikami, Photocatalytic O_2 evolution under visible light irradiation on $BiVO_4$ in aqueous $AgNO_3$ solution, Catal. Lett. 53 (1998) 229–230, https://doi.org/10.1023/A:1019034728816.

[62] F. Li, F. Yu, J. Du, Y. Wang, Y. Zhu, X. Li, L. Sun, Water splitting via decoupled photocatalytic water oxidation and electrochemical proton reduction mediated by electron-coupled-proton buffer, Chem. Asian J. 12 (2017) 2666–2669, https://doi.org/10.1002/asia.201701123.

[63] R. Li, F. Zhang, D. Wang, J. Yang, M. Li, J. Zhu, X. Zhou, H. Han, C. Li, Spatial separation of photogenerated electrons and holes among {010} and {110} crystal facets of $BiVO_4$, Nat. Commun. 4 (2013) 1432, https://doi.org/10.1038/ncomms2401.

[64] Y. Zhao, C. Ding, J. Zhu, W. Qin, X. Tao, F. Fan, R. Li, C. Li, A hydrogen farm strategy for scalable solar hydrogen production with particulate photocatalysts, Angew. Chem. Int. Ed. 59 (2020) 9653–9658, https://doi.org/10.1002/anie.202001438.

[65] V.J. Frilette, Preparation and characterization of bipolar ion exchange membranes, J. Phys. Chem. 60 (1956) 435–439, https://doi.org/10.1021/j150538a013.

[66] L. Chen, X. Dong, F. Wang, Y. Wang, Y. Xia, Base–acid hybrid water electrolysis, Chem. Commun. 52 (2016) 3147–3150, https://doi.org/10.1039/C5CC09642A.

[67] A. Ho, X. Zhou, L. Han, I. Sullivan, C. Karp, N.S. Lewis, C. Xiang, Decoupling $H_2(g)$ and $O_2(g)$ production in water splitting by a solar-driven $V^{3+}/^{2+}$(aq, H_2SO_4)|KOH(aq) cell, ACS Energy Lett. 4 (2019) 968–976, https://doi.org/10.1021/acsenergylett.9b00278.

[68] S. Goodwin, D.A. Walsh, Closed bipolar electrodes for spatial separation of H_2 and O_2 evolution during water electrolysis and the development of high-voltage fuel cells, ACS Appl. Mater. Interfaces 9 (2017) 23654–23661, https://doi.org/10.1021/acsami.7b04226.
[69] J. Lee, M. Kim, Y.-T. Kim, J. Choi, Asymmetric cell design for decoupled hydrogen and oxygen evolution paired with V(II)/V(III) redox mediator, Catal. Today 403 (2022) 67–73, https://doi.org/10.1016/j.cattod.2021.08.030.
[70] B. You, X. Liu, N. Jiang, Y. Sun, A general strategy for decoupled hydrogen production from water splitting by integrating oxidative biomass valorization, J. Am. Chem. Soc. 138 (2016) 13639–13646, https://doi.org/10.1021/jacs.6b07127.
[71] B. You, N. Jiang, X. Liu, Y. Sun, Simultaneous H_2 generation and biomass upgrading in water by an efficient noble-metal-free bifunctional electrocatalyst, Angew. Chem. Int. Ed. 55 (2016) 9913–9917, https://doi.org/10.1002/anie.201603798.
[72] W. Li, N. Jiang, B. Hu, X. Liu, F. Song, G. Han, T.J. Jordan, T.B. Hanson, T.L. Liu, Y. Sun, Electrolyzer design for flexible decoupled water splitting and organic upgrading with electron reservoirs, Chem 4 (2018) 637–649, https://doi.org/10.1016/j.chempr.2017.12.019.
[73] P. Peljo, H. Vrubel, V. Amstutz, J. Pandard, J. Morgado, A. Santasalo-Aarnio, D. Lloyd, F. Gumy, C.R. Dennison, K.E. Toghill, H.H. Girault, All-vanadium dual circuit redox flow battery for renewable hydrogen generation and desulfurisation, Green. Chem. 18 (2016) 1785–1797, https://doi.org/10.1039/C5GC02196K.
[74] Y. Ji, F. Zhang, M. Zhou, J. Yu, Q. Wang, Spatially decoupled hydrogen evolution in alkaline conditions with a redox targeting-based flow battery, Int. J. Hydrog. Energy 45 (2020) 18888–18894, https://doi.org/10.1016/j.ijhydene.2020.05.129.
[75] H. Bode, K. Dehmelt, J. Witte, Zur kenntnis der nickelhydroxidelektrode—i.Über das nickel (ii)-hydroxidhydrat, Electrochim. Acta 11 (1966) 1079–1087, https://doi.org/10.1016/0013-4686(66)80045-2.
[76] L. Chen, X. Dong, Y. Wang, Y. Xia, Separating hydrogen and oxygen evolution in alkaline water electrolysis using nickel hydroxide, Nat. Commun. 7 (2016) 11741, https://doi.org/10.1038/ncomms11741.
[77] A. Landman, H. Dotan, G.E. Shter, M. Wullenkord, A. Houaijia, A. Maljusch, G. S. Grader, A. Rothschild, Photoelectrochemical water splitting in separate oxygen and hydrogen cells, Nat. Mater. 16 (2017) 646–651, https://doi.org/10.1038/nmat4876.
[78] A. Landman, R. Halabi, P. Dias, H. Dotan, A. Mehlmann, G.E. Shter, M. Halabi, O. Naseraldeen, A. Mendes, G.S. Grader, A. Rothschild, Decoupled photoelectrochemical water splitting system for centralized hydrogen production, Joule 4 (2020) 448–471, https://doi.org/10.1016/j.joule.2019.12.006.
[79] H. Dotan, A. Landman, S.W. Sheehan, K.D. Malviya, G.E. Shter, D.A. Grave, Z. Arzi, N. Yehudai, M. Halabi, N. Gal, N. Hadari, C. Cohen, A. Rothschild, G. S. Grader, Decoupled hydrogen and oxygen evolution by a two-step electrochemical–chemical cycle for efficient overall water splitting, Nat. Energy 4 (2019) 786–795, https://doi.org/10.1038/s41560-019-0462-7.
[80] T. Brousse, D. Bélanger, J.W. Long, To be or not to be pseudocapacitive? J. Electrochem. Soc. 162 (2015) A5185–A5189, https://doi.org/10.1149/2.0201505jes.
[81] X. Yan, J. Biemolt, K. Zhao, Y. Zhao, X. Cao, Y. Yang, X. Wu, G. Rothenberg, N. Yan, A membrane-free flow electrolyzer operating at high current density using earth-abundant catalysts for water splitting, Nat. Commun. 12 (2021) 4143, https://doi.org/10.1038/s41467-021-24284-5.
[82] P.J. Nigrey, D. MacInnes, D.P. Nairns, A.G. MacDiarmid, A.J. Heeger, Lightweight rechargeable storage batteries using polyacetylene, $(CH)_x$ as the cathode-active material, J. Electrochem. Soc. 128 (1981) 1651, https://doi.org/10.1149/1.2127704.
[83] J. Kim, Y. Kim, J. Yoo, G. Kwon, Y. Ko, K. Kang, Organic batteries for a greener rechargeable world, Nat. Rev. Mater. 8 (2023) 54–70, https://doi.org/10.1038/s41578-022-00478-1.
[84] Y. Ma, X. Dong, Y. Wang, Y. Xia, Decoupling hydrogen and oxygen production in acidic water electrolysis using a polytriphenylamine-based battery electrode, Angew. Chem. Int. Ed. 57 (2018) 2904–2908, https://doi.org/10.1002/anie.201800436.
[85] Y. Ma, Z. Guo, X. Dong, Y. Wang, Y. Xia, Organic proton-buffer electrode to separate hydrogen and oxygen evolution in acid water electrolysis, Angew. Chem. Int. Ed. 58 (2019) 4622–4626, https://doi.org/10.1002/anie.201814625.
[86] M. Hou, L. Chen, Z. Guo, X. Dong, Y. Wang, Y. Xia, A clean and membrane-free chlor-alkali process with decoupled Cl_2 and H_2/NaOH production, Nat. Commun. 9 (2018) 438, https://doi.org/10.1038/s41467-018-02877-x.
[87] A. Zhao, F. Zhong, X. Feng, W. Chen, X. Ai, H. Yang, Y. Cao, A membrane-free and energy-efficient three-step chlor-alkali electrolysis with higher-purity naoh production, ACS Appl. Mater. Interfaces 11 (2019) 45126–45132, https://doi.org/10.1021/acsami.9b16754.
[88] M. Guo, J. Zhan, Z. Wang, X. Wang, Z. Dai, T. Wang, Supercapacitors as redox mediators for decoupled water splitting, Chin. Chem. Lett. 34 (2023) 107709, https://doi.org/10.1016/j.cclet.2022.07.052.
[89] Z. Liu, G. Zhang, K. Zhang, H. Lan, H. Liu, J. Qu, Low electronegativity mn bulk doping intensifies charge storage of Ni_2P redox shuttle for membrane-free water electrolysis, J. Mater. Chem. A 8 (2020) 4073–4082, https://doi.org/10.1039/C9TA10213B.
[90] S. Musikajaroen, S. Polin, S. Sattayaporn, W. Jindata, W. Saenrang, P. Kidkhunthod, H. Nakajima, T. Butburee, N. Chanlek, W. Meevasana, Photoenhanced water electrolysis in separate O_2 and H_2 cells using pseudocapacitive electrodes, ACS Omega 6 (2021) 19647–19655, https://doi.org/10.1021/acsomega.1c02305.
[91] J. Wang, L. Ji, X. Teng, Y. Liu, L. Guo, Z. Chen, Decoupling half-reactions of electrolytic water splitting by integrating a polyaniline electrode, J. Mater. Chem. A 7 (2019) 13149–13153, https://doi.org/10.1039/C9TA03285A.
[92] M. Guo, L. Wang, J. Zhan, X. Jiao, D. Chen, T. Wang, A novel design of an electrolyser using a trifunctional (HER/OER/OORR) electrocatalyst for decoupled H_2/O_2 generation and solar to hydrogen conversion, J. Mater. Chem. A 8 (2020) 16609–16615, https://doi.org/10.1039/D0TA05102K.
[93] C. Peng, D. Hu, G.Z. Chen, Achieving low voltage half electrolysis with a supercapacitor electrode, Energy Environ. Sci. 7 (2014) 1018–1022, https://doi.org/10.1039/c3ee43817a.
[94] Y. Chen, G.Z. Chen, A half-electrolysis water instrument with one reaction electrode, (2019) China Patent 2019 10155530.6.
[95] Y. Chen, G.Z. Chen, A half-electrolysis water instrument with two reaction electrodes, (2019) China Patent 2019 10155553.7.
[96] Y. Chen, G.Z. Chen, Half-electrolysis of water with the aid of a supercapacitor electrode, ACS Appl. Energy Mater. 6 (2023) 6104–6110, https://doi.org/10.1021/acsaem.3c00615.
[97] H. Xie, Z. Zhao, T. Liu, Y. Wu, C. Lan, W. Jiang, L. Zhu, Y. Wang, D. Yang, Z. Shao, A membrane-based seawater electrolyser for hydrogen generation, Nature 612 (2022) 673–678, https://doi.org/10.1038/s41586-022-05379-5.
[98] J. Guo, Y. Zheng, Z. Hu, C. Zheng, J. Mao, K. Du, M. Jaroniec, S.-Z. Qiao, T. Ling, Direct seawater electrolysis by adjusting the local reaction environment of a catalyst, Nat. Energy 8 (2023) 264–272, https://doi.org/10.1038/s41560-023-01195-x.
[99] K. Veeramani, G. Janani, J. Kim, S. Surendran, J. Lim, S.C. Jesudass, S. Mahadik, H. lee, T.-H. Kim, J.K. Kim, U. Sim, Hydrogen and value-added products yield from hybrid water electrolysis: a critical review on recent developments, Renew. Sust. Energy Rev. 177 (2023) 113227, https://doi.org/10.1016/j.rser.2023.113227.
[100] H. Choi, S. Surendran, D. Kim, Y. Lim, J. Lim, J. Park, J.K. Kim, M.-K. Han, U. Sim, Boosting eco-friendly hydrogen generation by urea-assisted water electrolysis using spinel M_2GeO_4 (M = Fe, Co) as an active electrocatalyst, Environ. Sci. Nano 8 (2021) 3110–3121, https://doi.org/10.1039/D1EN00529D.
[101] Y. Lim, S. Surendran, W. So, S. Shanmugapriya, C. Jo, G. Janani, H. Choi, H. S. Han, H. Choi, Y.-H. Yun, T.-H. Kim, M.-J. Kim, K. Jin, J.K. Kim, U. Sim, In situ decorated Cu_2FeSnS_4 nanosheet arrays for low voltage hydrogen production through the ammonia oxidation reaction, Mater. Chem. Front. 7 (2023) 5843–5857, https://doi.org/10.1039/D3QM00291H.
[102] B. You, Y. Sun, Innovative strategies for electrocatalytic water splitting, Acc. Chem. Res. 51 (2018) 1571–1580, https://doi.org/10.1021/acs.accounts.8b00002.
[103] Z. Zhu, X. Zhao, B.Y. Xia, B. You, Efficient noble-metal-free integration electrolysis for solar H_2 and supercapacitor electrode coproduction in acidic water, ChemSusChem (2024) e202301213, https://doi.org/10.1002/cssc.202301213.

Yao Chen (ORCID: 0000–0003–0147–8156) received his BSc from Hubei University of Automotive Technology in 2006, obtained his MSc from Huazhong University of Science and Technology under Prof. Jian Li's supervision in 2008 and PhD degree from Institute of Electrical Engineering, Chinese Academy of Sciences under Prof. Yanwei Ma's supervision in 2012. He then completed his postdoc researches in IFW Dresden, Germany, together with Prof. Oliver G. Schmidt and in AIST Kansai, Japan with Prof. Qiang Xu. After that, he joined Wuhan University of Science and Technology as an instructor in 2015 and became an associate professor in 2022. He has been mainly engaged in researches on carbon-based electrochemical energy storage devices, heterogeneous catalysis and electrocatalysis.

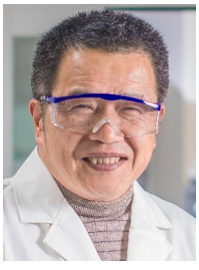

George Zheng Chen (ORCID: 0000–0002–5589–5767) graduated from Jiujiang Teachers Training College with a Diploma in Chemistry in 1981, Fujian Normal University with the MSc in Physical Chemistry (Electrochemistry) in 1985, and the University of London with the PhD and DIC in Physical Chemistry (Electrochemistry) in 1992. After contracted work in the Universities of Oxford, Leeds and Cambridge, he joined the University of Nottingham in 2003 as Reader, and has been Professor since 2009. He was Specially Invited Professor of Wuhan University of Science and Technology between 2015 and 2019. His ongoing research aims at electrochemical and liquid salts innovations for materials, energy and environment.